

SOLID STATE PHYSICS
FACULTY OF ENGINEERING
LUND UNIVERSITY

MASTER THESIS

Detection of gunshot residue and explosives using
hybrid graphene/quantum dot based sensors

Elsa DE GEER

Supervisors: Dan HESSMAN & Qin WANG & Ying FU

Examiner: Carina FASTH

December 21, 2016



LUND
UNIVERSITY

Abstract

This master thesis investigates the use of chemically exfoliated graphene, CdSe/CdS/ZnS quantum dots and graphene quantum dots for fluorescence based detection of gunshot residue and explosives. Specifically, nitroglycerine is chosen as the target substance in gunshot residue and the nitroaromatic compounds trinitrotoluene and dinitrotoluene are chosen as target explosives.

The experimental work is divided into three parts where the first one is an investigation of the quenching of semiconductor quantum dot fluorescence by graphene. The results show that graphene is an efficient quencher, and it is probable that quenching takes place without the fluorescing and quenching agents being in contact, through either Förster resonance energy transfer or nanometal surface energy transfer.

The second part is a study of how nitroaromatic molecules quench the fluorescence from graphene quantum dots. The results indicate that the solvent of the nitroaromatics passivates the functional groups which reduces the quenching efficiency. Nevertheless, it is concluded that the nitroaromatics quench the fluorescence. It is possible that the quenching mechanism is photoinduced charge transfer.

The last part of the experimental work investigates the influence of nitroaromatics on the graphene and semiconductor quantum dot hybrid from the first part. It is shown that nitroaromatics further quench the fluorescence of the quantum dots in the hybrid structure, possibly by photoinduced charge transfer or by reacting with the surface coating of the quantum dots and thereby introducing de-excitation through surface states.

Acknowledgements

I would like to thank my supervisors, Dr. Qin Wang, Prof. Ying Fu and Ass. Prof. Dan Hessman. At KTH, Prof. Joydeep Dutta, Dr. Abdusalam Uheida, Dr. Yichen Zhao and Wei Zhao for access to, and guidance in, the lab. The staff at Acreo, one and all. A special thank to Mikael Karlsson for listening to my rants and always giving useful input.

Contents

Abstract	1
Acknowledgements	1
List of Acronyms	3
1 Introduction	4
1.1 Background	4
1.2 Outline and aim	9
2 Theory	11
2.1 Organic chemistry	11
2.2 Fluorescing semiconductor quantum dots	14
2.3 Graphene and rGO	15
2.4 Graphene quantum dots	17
2.5 Fluorescence quenching	18
2.6 Targets for detection	26
2.7 Instruments	28
3 Methods and Materials	34
3.1 GSR sampling	34
3.2 Synthesis and characterization of rGO	35
3.3 QD fluorescence quenching with rGO	35
3.4 Synthesis and characterization of GQDs	35
3.5 GQD fluorescence quenching by nitroaromatic compounds	36
3.6 Turn-on fluorescence by addition of nitroaromatics to graphene- quenched semiconductor QDs	36
4 Results and discussion	37
4.1 SEM-EDS of gunshot residue	37
4.2 Characterization of rGO	40
4.3 Semiconductor QD characterization	42
4.4 Quenching of semiconductor QD fluorescence with rGO	44
4.5 Graphene quantum dot characterization	48

4.6	Quenching of GQD fluorescence with nitroaromatic compounds .	52
4.7	Detection of nitroaromatics with a hybrid of semiconductor QDs and rGO	56
5	Conclusion and outlook	60
5.1	Summary and conclusion	60
5.2	Outlook	62
A	Appendix A, Synthesis of rGO	68
B	Appendix B, Synthesis of GQDs	70
C	Appendix C, Instruments	72
C.1	FTIR	72
C.2	UV-VIS	74
C.3	PL	74
C.4	SEM-EDS	74

Acronyms

3-MPA 3-mercaptopropionic acid.

AA Ascorbic acid.

DNT Dinitrotoluene.

FRET Förster resonance energy transfer.

FTIR Fourier transform infra-red spectroscopy.

GO Graphene oxide.

GQDs Graphene quantum dots.

GSR Gunshot residue.

MAH Microwave-assisted hydrothermal.

NSET Nanometal surface energy transfer.

PL Photoluminescence.

PLE Photoluminescence excitation.

QDs Quantum dots.

rGO Reduced graphene oxide.

SEM-EDS Scanning electron microscopy - energy dispersive x-ray spectroscopy.

TNT Trinitrotoluene.

UV-VIS Ultraviolet-visible spectroscopy.

1 Introduction

1.1 Background

In forensic science, one challenge concerns the detection of small amounts of chemical compounds on crime sites and suspects. Today, advanced and expensive lab equipment yield good results regarding both both sensitivity (ability to detect small amounts) and selectivity (ability to distinguish between different substances). However, sending samples to a lab is cumbersome, time-consuming and costly. This opens up the field for smaller, more agile detectors.

Nanotechnology can be used in the design of these detectors. In this master thesis project, one specific approach is investigated: fluorescence based detection. Quantum dots (QDs) can be functionalized so that the fluorescence intensity changes if they are in contact with specific compounds. By measuring the fluorescence intensity, both qualitative and quantitative information can be obtained.

More specifically, the detection can be done in two ways. Turn-off detection means that the presence of the sought-after compound results in a decreased fluorescence intensity. The action of decreasing fluorescence intensity is called quenching. The second alternative is called turn-on fluorescence. In this case, the fluorescing agent is quenched in the ground state, and the presence of the sought after compound results in an increase in fluorescence. Although the turn-off fluorescence approach is simpler, the turn-on detection approach can provide a higher selectivity and sensitivity as there are fewer error sources (see section 2.5 for further explanation).

In this chapter, an introduction to areas of importance for the project is given. First, an introduction to forensic science and the sought-after compounds, gunshot residue and explosives, is given. Thereafter, the materials used in the detector are presented, starting with graphene and its function as a fluorescence quencher and then moving on to semiconductor and carbon based QDs.

1.1.1 Forensic science

Forensic science is an umbrella term for scientific techniques used in criminal and civil investigations [1]. It concerns the collection, preservation and analysis of evidence from crimes. Wikipedia lists over 40 subdivisions of forensic science, ranging from analysis of mobile phone data to forensic entomology - the study of insects [2].

Many areas of forensic science involve chemical substances that could be detected both qualitatively and quantitatively with fluorescence-based biosensors. For example, by the selectivity of RNA-strands, a quick indication of a matching DNA sample can be achieved [3]. QDs can be used in nanosensors for drug detection [4]. There is a lot of research on biology-inspired systems for detection of explosives [5], many of which can be converted to fluorescence based detection. Gunshot residue (GSR) contains a large amount of both organic and inorganic particles, which can be detected and identified using protein based aptamers in nanobiosensors [6].

National Forensic Center and Swedish Defence Research Agency (Totalförsvarets forskningsinstitut) have expressed an interest in easy-to-use and portable detectors for GSR and explosive, that can be used in the field by policemen and/or military. GSR and explosive samples are also obtainable and don't require additional licensing. Therefore, this project is focused on the detection of gunshot residue and explosives.

1.1.2 Gunshot residue

When a firearm is discharged, the bullet isn't the only thing that leaves the gun: many other substances are also released. This includes both burnt and unburnt products from primer and propellant, particles from grease, lubricants, metals from the cartridge and the weapon itself [7, 8, 9]. In the figure below, ammunition for a typical gun is illustrated. It consists of a cartridge packed with bullet, propellant and primer. When the primer is impacted with sufficient force, it produces enough heat to ignite the propellant, which is the explosive fuel that "fires" away the bullet. The cartridge is the packaging of the primer, propellant and bullet.

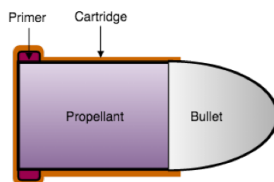


Figure 1.1: Illustration of the typical components of ammunition: a cartridge packed with bullet, propellant and primer.

Up until today, the single most common method for detection of GSR has been through residues from the primer: a combination of lead, barium and antimony has been considered unique for GSR. Due to health concerns, heavy metal free primers are increasingly common. This renders the conventional detection method of Pb, Ba, Sb less useful as there will no longer be any lead in the residue and Ba-Sb is not unique for GSR.

An alternative to the detection of Pb, Ba, Sb is to focus on the organic components of GSR. These are mainly unburnt and partially burnt propellant and firearm lubricant [7, 8]. Lubricant and other additives often differ between manufacturers, but the propellant components are quite standardized. It usually involves one of the following three:

- Nitrocellulose, which is also called single base powder
- nitrocellulose combined with a small quantity of nitroglycerine, which is also called double base powder
- nitrocellulose, nitroglycerine and nitroguanidine, which is also called triple base powder.

In this project, the focus has been on the detection of organic GSR.

1.1.3 Explosives

Because of an increased threat to public safety and homeland security, the interest in explosive detection has increased both regarding new methods and improvements of current techniques in terms of cost, speed, sensitivity and simplicity. Furthermore, due to a long term use of explosives in warfare, applications in efficient land and sea mine detection as well as monitoring of long-term environmental effects of explosives is needed. For example, Trinitrotoluene (TNT) is considered an environmental pollutant [10, 11]. Lately, several articles using fluorescence based methods for detection of explosives have been published [11, 12].

There are many explosive compounds, some of the more common are:

- Nitroaromatics, e.g. TNT, 2,4,6-trinitrotoluene, and DNT, dinitrotoluene
- TNP, Trinitrophenol
- RDX, Cyclotrimethylenetrinitroamine
- PETN, Pentaerythritol tetranitrate
- Nitroglycerine
- Peroxide based explosives
- Ammonium nitrates
- Chlorate based explosives

Detection of nitroaromatic explosives has been the focus of this project.

1.1.4 Current methods for detection of GSR and explosives

Almost any analytical chemistry method can be used to obtain information about a GSR or explosive sample. Here, some of the more common methods are listed.

Scanning electron microscopy - energy dispersive x-ray spectroscopy (SEM-EDS): This is the most common method for determining if a sample contains gunshot residues. Firstly, particles with a morphological resemblance to GSR are identified using SEM, and the composition of said particle is then determined using EDS [7, 9]. By targeting particles in GSR instead of doing bulk analysis, the specificity increases as the composition of the identified combustion particles can be analyzed, without detection of background compounds. Although a good method for GSR analysis, it is time-consuming and expensive. Because the equipment is bench bound, analysis has to be conducted in laboratories. With the increased use of lead-free ammunition, the characterization ability of SEM-EDS will decrease.

Ion Mobility Spectrometry (IMS): IMS is a widely used method for detection of explosives [10]. It gives both qualitative and quantitative information and it has a low detection limit. The sample is ionized and the mobility of the ions in a carrier gas is measured under an electric field applied. Disadvantages include radioactive ionization sources and bulky, bench-bound instruments. IMS is commonly used at e.g. airports.

Mass Spectrometry (MS): MS is another commonly used instrument [10]. It is fast and can specifically identify many substances. In MS, the substances are separated according to their mass/charge ratio, for example with the time-of-flight method: the ions are accelerated by an electric field, meaning that the kinetic energy depends on the charge. The time it takes for them to travel a specific distance is measured. As the speed depends on the mass of the particle, a mass/charge ratio is obtained. The high cost of the setup used to limit the use, but cheaper and less bulky machines are becoming available [13].

Liquid Chromatography-Mass Spectrometry (LC-MS): In LC-MS, high performance liquid chromatography is added as a step prior to the aforementioned MS. Liquid chromatography is a separation technique where the a solvent containing the sought-after compound is passed through a column. The column contains some sort of absorbent media, usually in the shape of granulates, and the solution is under pressure. Different components in the sought-after compound will be affected differently by the absorbent, resulting in different flow rates, and thereby separation. The LC separation is followed by MS. This method can provide good specificity, but just as with the methods mentioned above, the setup is bulky, bench-bound and expensive [13].

In summary, SEM-EDS, the conventional method for GSR detection, remains costly and cumbersome, and the accuracy will decrease substantially with heavy metal free primers. There is clearly room for cheaper, more agile methods for analysis of GSR. Consistently, current instruments for detection of explosives are expensive and bench-bound, once again giving room for cheaper tools that can be transported into the field. With this said, the demand for selectivity and sensitivity cannot be compromised: false-yes results is a no-no in forensic applications, and the amounts of GSR or explosives present on sites are usually very small.

1.1.5 Graphene

Graphene is a 2-dimensional material consisting of carbon atoms that are packed in a honeycomb structure [14, 15]. Although theoretically studied for a long time, the first experimental discovery of free standing graphene sheets was achieved by Geim and Novoselov in 2004, and was later awarded with the Nobel prize in 2010. The material is hyped due to its many groundbreaking properties, e.g. the high electron mobility and elasticity. All of these properties have potential applications in an enormous range of areas; cell phone screens, energy harvesting and biomedicine. However, before graphene products gain a large market, graphene manufacturing needs to be industrialized and standardized and the cost has to be reduced [16].

In general, graphene production methods can be divided into two categories, bottom-up and top-down synthesis [17]. The first one consists of growing graphene sheets from scratch which results in pristine single-layer graphene. The second approach seeks to exfoliate layers of graphene from graphite, either mechanically or chemically. In terms of production cost and possibility of industrialization, the top-down chemical methods have come the furthest, and today large amounts can be produced at a rather low cost.

Chemically derived graphene is a suitable material for fluorescence quenching due to its high optical absorption (for being only a few atom layers) over a wide wavelength range [14, 15].

The graphene produced through oxidation-exfoliation-reduction of graphite consists of small sheets, usually varying in thickness and size. It is commonly used in composites, conductive inks and batteries [18, 17]. Unlike pristine graphene, there are defects and some remaining functional groups in rGO. These can be used for functionalization, which is useful in biomedical and chemical sensor applications.

1.1.6 Quantum dots

One type of QDs are semiconductor particles with size in the nanometer-range. They are fluorescent, meaning that they emit light upon photo-excitation. QDs can be used for bio-labeling, as light emitting diodes and in fluorescence sensing applications [19]. For example, Liu et al. use QDs for detection of Vitamin E [20], and Li et al. describe a turn-on detector for lead based on QDs and graphene oxide [6].

Graphene quantum dots (GQDs) are graphene sheets with size smaller than 100 nm. At this size, confinement can lead to fluorescence [21]. Other sources of fluorescence are the defects and functional groups on edges and surface. There are many health concerns regarding semiconductor QDs as they often contain toxic compounds, e.g. Cadmium. The use of GQDs and other fluorescing carbon nanoparticles is an intriguing alternative, as they might be completely bio compatible [21] and still have similar fluorescence properties to regular, semiconductor QDs.

1.2 Outline and aim

The work in this master thesis was a pilot project at Acreo Swedish ICT on the use of graphene and QD based fluorescence sensors for forensic applications. As this is a very broad subject, I started the project with deciding on some further restrictions and more specific goals. Firstly, I chose GSR and explosive substances as targets for the sensor. Blood samples was another alternative, but the process of getting the licensing and permissions needed to handle blood samples would have taken too long. The same applied to investigation of drug samples. In addition, both the National Forensic Center and Swedish Defence Research Agency expressed a wish for new and improved sensing systems for GSR and explosives.

Secondly, I made a very coarse outline for the project:

- a investigate current methods for detection of GSR and explosives
- b specify requirements for future detection systems
- c proof-of-concept test of sensor alternatives.

Through comprehensive literature study and guidance from numerous people, I later decided to investigate three sensor alternatives based on graphene and fluorescing quantum dots:

- a Reduced graphene oxide (rGO) and QDs functionalized to be sensitive for specific targets. In the ground state the QD fluorescence is quenched by the rGO. Upon addition of target, the rGO-QD-distance increases and the fluorescence is recovered, thereby achieving a turn-on fluorescence signal.

I tested the quenching capability of rGO on the QD fluorescence, but I did not perform any functionalization of the QDs.

- b Fluorescence turn-off of GQD fluorescence by nitroaromatics. This model relies on a binding affinity between the graphene structure and nitroaromatic compounds. I tested this type of fluorescence quenching with several types of nitroaromatic compounds.
- c Fluorescence turn-on by nitroaromatics using rGO + QDs. Here, the idea was for the nitro-aromatics to *kick out* the QDs from the vicinity of the graphene, and thereby yielding an increase in fluorescence. When testing this, I discovered that nitroaromatics quench semiconductor QD fluorescence as well. Therefore, the concept doesn't work.

2 Theory

In this chapter I summarize the theory used in the design of the sensing mechanisms and the models that are used in the analysis of the results. This starts with a short introduction to organic chemistry, and is followed by detailed descriptions of the materials that are used. The concept of fluorescence quenching together with models that can be used in the characterization of quenching statics and dynamics are presented, and then, lastly, the different means for obtaining selective detection are described.

2.1 Organic chemistry

Organic chemistry is a subcategory of chemistry that studies the properties of organic compounds, e.g. structure and reaction mechanisms. Basic knowledge of organic chemistry is useful for many areas of this project, for example the synthesis of rGO and the selectivity mechanism between graphene and nitroaromatic explosives.

2.1.1 Atomic orbitals

Electrons in atoms are located in orbitals around the nucleus [22]. The orbitals describe the probability of finding an electron at a specific spot in relation to the nucleus. They are labeled s, p, d and f and differ in shape, energy and orientation. The orbitals are grouped together in shells of different energy. The shells are labeled $n = 1, 2, 3, \dots$

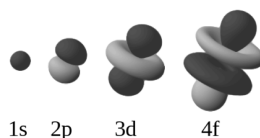


Figure 2.1: Shape of s, p, d and f atomic orbitals. Light and dark gray corresponds to the reverse phase of the electron wavefunction.

The shapes of the different atomic orbitals are illustrated in figure 2.1. The s orbital is centered in the origin, with a low probability of finding the electron far away from the nucleus. There are three p-orbitals, p_x , p_y and p_z , with the same shape and energy but different orientation, so that they are perpendicular to one another. There is room for two electrons in each orbital, one of each spin [22].

2.1.2 Molecular orbitals

Atoms form molecules because it lowers the total energy of the systems. In molecules, the electrons of the different atomic orbitals combine and form new orbital shapes. This is sometimes called molecular hybridization. Covalent bonds are either formed between these hybridized orbitals or regular atomic orbitals. Carbon, which has four valence electrons ($2s^2$, $2p^2$) can hybridize in three different ways, as is illustrated in figure 2.2. The first figure shows the sp hybridization, where the s orbital mixes with one of the p orbitals. The remaining two p orbitals are non-hybridized. The second image shows the shape of the sp^2 hybridization, where the s-orbital combines with two of the p orbitals. The third image describes the sp^3 hybridization, where all three p orbitals take part in the formation of new molecular orbitals.

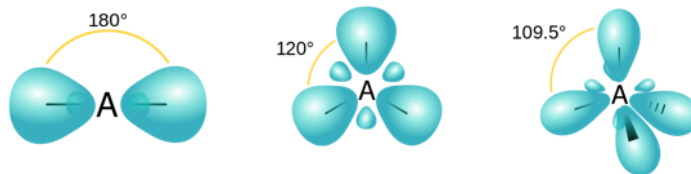


Figure 2.2: Illustration of hybridization in carbon: sp, sp^2 and sp^3 . Images by José Fernando Melero, CC-BY-SA 3.0.

In graphene, the carbon is sp^2 -hybridized. The three electrons in the hybridized orbitals bond to electrons in corresponding orbitals of other atoms, forming three σ -bonds. The orientation of the molecular orbitals determine the orientation of the bonds, and the directions of the sp^2 molecular orbitals explain the 2D property and hexagonal structure of graphene [22]. The fourth electron, which is in a non-hybridized 2p orbital, can form a π bond with a 2p-electron in an adjacent carbon atom. This is illustrated to the left in figure 2.3. In an aromatic ring, the 2p-electrons in the six carbon atoms form a conjugated π -bond, which covers the whole ring. This is illustrated to the right in figure 2.3. The delocalized electrons in the conjugated π -bond produce a high stability in aromatic molecules [22].

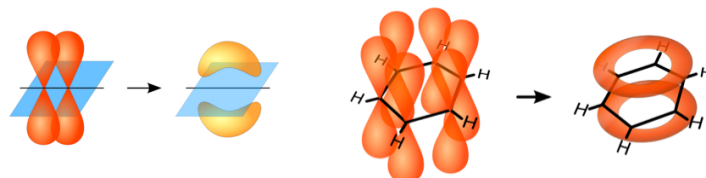


Figure 2.3: Illustration of the formation of a π -bond (left) and the delocalized electrons in a conjugated π -bond in an aromatic ring (right). Image by Vladsinger, CC-BY-SA 3.0.

2.1.3 Bonding and antibonding

Electron orbitals in molecules can be grouped into bonding, non-bonding and antibonding orbitals, as illustrated in figure 2.4. Bonding orbitals are those that participate in the creation of bonds between atoms in a molecule. They have lower energy than the atomic orbitals that combine to produce them. In the carbon example above, the hybridized orbitals and subsequent covalent bonds will result in a lower energy of the molecule compared to the non-bonded atom.

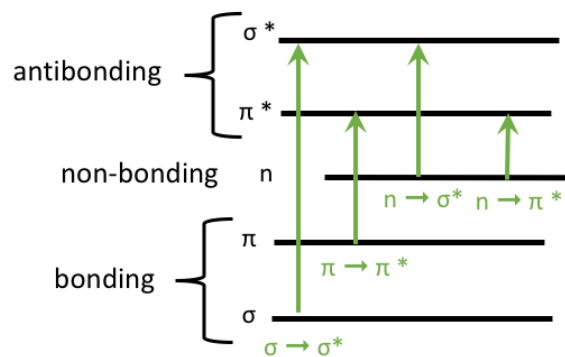


Figure 2.4: Bonding, antibonding and non-bonding orbitals. The possible transitions are marked with green arrows.

For each of the bonding orbitals, there is a corresponding antibonding orbital. In the above example, the σ and π orbitals have corresponding antibonding orbitals, denoted σ^* and π^* [23]. The energy is higher in the antibonding orbitals because the electron density between the two bonding atoms is lower compared to both the bonding and non-bonding case.

The non-bonding orbitals, denoted with an n, consist of electrons that don't take part in bond formation. In the bond between two carbon atoms in graphene, there are no non-bonding orbitals since all valence electrons participate in the bonding. However, in e.g. a C-O bond there are non-bonded valence electrons originating from the oxygen atom.

When a molecule absorbs light in the UV-VIS range, electrons are excited from bonding (σ or π) or non-bonding orbitals (n) to antibonding orbitals (σ^* or π^*), as illustrated in figure 2.4. These transitions are further described in section 2.7.2.

2.2 Fluorescing semiconductor quantum dots

QDs are semiconductor particles with size in the nano-range [19]. At this scale, optical and electronic properties are determined by quantum physics. Electrons in QDs can be described by quantum wave functions, giving rise to discrete electronic states similar to those in atoms and molecules. The distance between the energy levels in QDs is size dependent, making the emission wavelength tunable. QDs are sometimes called artificial atoms due to the similarities in energy structure. Figure 2.5 shows the conduction and valence band in semiconductor QDs, and illustrates how fluorescence works.

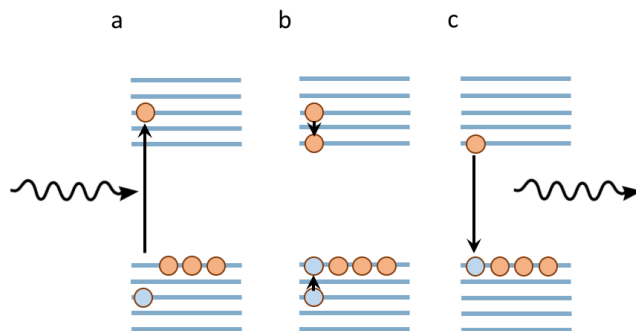


Figure 2.5: Schematic sketch of excitation (a), relaxation (b) and fluorescence (c) in semiconductor quantum dot with discrete energy levels.

Incoming light excites an electron in the valence band to the conduction band. This leaves a hole in the valence band. The electron-hole pair is called an exciton. As there are several available energy levels in the conduction band, the excitation energy can be larger than the band gap. The electron will relax vibrationally to the lowest conduction band energy. Thereafter, the electron and hole pair can recombine, and in doing so the excess energy will be emitted as a photon. As illustrated above, the emitted photon will have a lower energy

than the excitation energy, and the energy difference has turned into vibrational energy (heat).

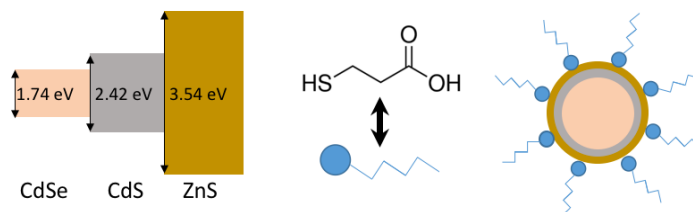


Figure 2.6: To the left: bandgaps of the different layers in the QD. Center: Molecular structure of 3-MPA. To the right: core-shell-shell QD coated with 3-MPA.

In this project, the semiconductor QDs are CdSe/CdS/ZnS core-shell-shell quantum dots from SciLifeLab in Stockholm. The shells act as surface passivating layers, reducing non-radiative recombination of QD excitons through surface states. The QDs are illustrated in figure 2.6, where the bandgaps of the QD core and shells are shown. The QDs are coated in 3-mercaptopropionic acid (3-MPA), which is shown in the same figure. The 3-MPA consists of a carbon chain with two functional groups, a carboxyl group and a thiol (S-H). The S atoms in the thiol bond to the Zn atoms in the QD shell, and leaves the hydrophilic carboxyl groups as the outer layer. The 3-MPA coated QDs are thereby soluble in water [19].

2.3 Graphene and rGO

From a manufacturing point of view, graphene can be divided into two main categories: top-down and bottom-up graphene. The latter can result in large sheets of pristine graphene with few defects. However, it is expensive and difficult to scale to industrial quantities. The alternative, top-down graphene, is produced through the exfoliation of graphite. The "first" graphene, discovered by Geim and Novoselov in 2004, was produced by mechanical exfoliation [24]. A more scalable method is chemical oxidation, exfoliation and reduction of graphite [17]. I will focus on this type of graphene because that is what is used in the experiments.

The conventional method of oxidation when producing graphene is through Hummers method and modifications thereof [25]. During the oxidation of graphite, oxygen-containing functional groups appear on the surface of the graphite layers. This increases the distance between the layers which in turn reduces the van der Waals-forces binding them together. The oxidation is followed by some sort of exfoliation, commonly through stirring or ultrasonication in a polar media (an organic solution or water). The exfoliation separates the graphite

oxide layers, and the result is mono- or few-layer Graphene oxide (GO); layers of graphene with oxygen containing functional groups. To obtain graphene, the GO is reduced, which means that the functional groups are removed. There are many ways to do the reduction, both thermal, electrochemical and chemical processes [17].

The functional groups that are present in graphite oxide and graphene oxide are mostly

- epoxide groups, also known as epoxy bridges (-O-)
- hydroxyl groups (-OH)
- carboxyl groups (-COOH)
- carbonyl groups (=O)

Epoxy bridges and hydroxyl groups are common on surfaces, whereas carboxyl and carbonyl groups are present at the edges of the graphite/graphene flakes [17].

The properties of the rGO (conductivity, structure, morphology etc.) will vary a lot depending on the choice of reduction method. When comparing rGO to pristine graphene, there will be many more defects in the rGO. This is partially because of the functional groups present during the oxidation-reduction process, and partially because ultrasonication leads to structural damages in the sheets. Ultrasonication also tears some of the rGO sheets into smaller fragments.

A common chemical reducing agent of GO is hydrazine, but in the search for less dangerous and toxic reducing agent, other alternatives have been reported. Ascorbic acid (AA), also known as vitamin C, is an essential nutrient commonly found in food, and an anti-oxidant. It has been reported as a good, "green", substitute to hydrazine and I have therefore used AA as reducing agent [26, 27].

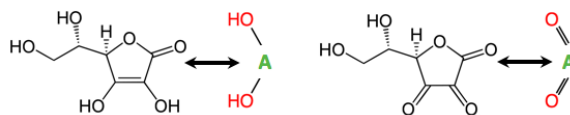


Figure 2.7: Chemical structure and simplified structure of ascorbic acid (left) and dehydroascorbic acid (right). The simplified version is used in the image below, when describing the process for reducing GO.

The chemical structure of AA is shown in figure 2.7. The reduction process proposed by Fernández-Merino et. al is a double nucleophilic substitution reaction with the hydroxyl or epoxide groups, which is illustrated in figure 2.8 [26]. The protons in AA have a high binding affinity to oxygen containing functional groups. As shown in the first step, the AA will perform a so-called

backside nucleophilic attack, resulting in the release of a water molecule. The second step shows the same event for the second hydroxyl group of the AA. In the third step, the AA is thermally eliminated resulting in dehydroascorbic acid and reduced graphene.

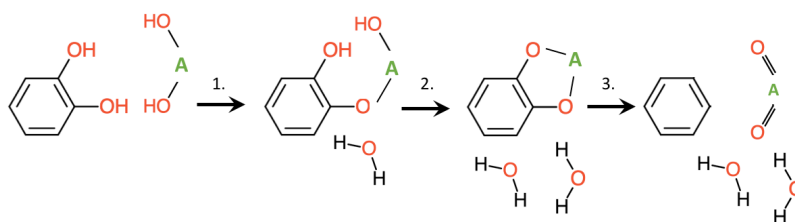


Figure 2.8: Schematic sketch of the reduction process of graphene oxide with AA. For clarity, only one graphene ring and the simplified structure of AA is shown. Step 1: The AA performs a backside nucleophilic attack, leading to the deprotonation of an hydroxyl group and the release of a water molecule. Step 2: The same reaction for the second hydroxyl group. Step 3: Thermal elimination of the deprotonated AA (dehydroascorbic acid).

The progress of the reduction process for rGO can be monitored by absorption spectroscopy; the absorption peak red-shifts throughout the reduction starting at 230 nm and ending up around 270 nm [27]. This is due to differences in the intensity and energy of the $\pi - \pi^*$ and $n - \pi^*$ transitions in rGO and GO and will be further described in section 2.7.2.

2.4 Graphene quantum dots

Pristine graphene is a zero band gap material, and therefore doesn't exhibit any luminescence. By reducing the size of graphene flakes, confinement can be achieved, and thereby quantized energy levels [21]. As the edge-to-surface-ratio increases for smaller flakes, edge effects can also add to new optical properties of graphene. In rGO, both functional groups and surface defects are present, and these can give rise to luminescence through edge/surface states. The fluorescent semiconductor QDs used in this project, as well as most QDs used in applications today, contain toxic metals (e.g. Cadmium). GQDs with similar properties have no observed toxicity and would thus have a great advantage over conventional QDs in all applications, above all in biomedicine [21].

Synthesis of GQDs can be divided into two main routes: top-down and bottom-up. Top down-synthesis generally consists of breaking larger graphene flakes into smaller fragments. I will focus on a bottom-up microwave technique. Microwave-assisted hydrothermal (MAH) methods are a convenient and fast and can also shorten reaction time and increase yield when synthesizing regular rGO [21].

Tang et al. [28] demonstrate a facile synthesis method where microwave heating of glucose results in GQDs. The proposed reaction mechanism is as follows: First, the glucose is dehydrated and a core with C=C bonds is formed. As new glucose molecules reach the surface of the core, new C=C bonds are created by dehydration. The hydrothermal heating induces a high pressure in the vessel which makes the C=C bonds nicely arranged and assists the crystalline property of the growing particles. The surface of the particles contains functional groups (e.g. -OH, -COOH, -C-H and -C-O-R, where R is a another carbon chain), which act as a passivating layer and make the GQDs hydrophilic. These surface groups, together with lattice defects, may also give rise to fluorescence.

The absorption of GQDs usually extends deep into the UV range, with two main peaks originating from C=C and C=O transitions; $\pi \rightarrow \pi^*$ in C=C and C=O and $n \rightarrow \pi^*$ in C=O (see figure 2.4). Depending on the type of functional group, the n levels have different energies which results in a range of $n\pi^*$ transitions. There is also a variation in the π and π^* energies depending on adjacent atoms, which gives a broadened $\pi \rightarrow \pi^*$ band [28]. I return to the absorption transitions in section 2.7.2.

The photoluminescence of the GQDs produced with the microwave method by [28] is size-independent.

Another example of a fluorescent carbon material is carbon dots. GQDs can be considered a sub-category of carbon dots, with the important characteristic of having graphene lattice. Theoretically, GQDs only contain C and H, but all reported GQDs are partially oxidized, with edge and surface groups such as hydroxyls, carboxyls, epoxy bridges and carbonyls. Carbon dots are usually defined as carbon particles with diameter below 10 nm and almost spherical geometry. GQDs are graphene sheets smaller than 100 nm, consisting of less than 10 layers of graphene. Reported size average of GQDs is below 10 nm, so the size cannot be used for determining the type of carbon nanoparticle. The only remaining mean to distinguish between the two is by studying the carbon lattice itself.

2.5 Fluorescence quenching

Fluorescence is defined as the emission of light after absorption of light (or other electromagnetic radiation). The decrease of fluorescence is called quenching. In this project, I study the possibility to use fluorescence quenching as a way to detect GSR and explosives. One way to do so is by using the target (e.g. nitroaromic explosives) as a quenching agent, and thus only having the fluorescing agent present in the sensor. Another way to do this is to start out with quenched fluorescing agents that are connected to an antibody, or something else that binds to the target. This is illustrated in figure 2.9. When the antibody binds to the target, the distance between the QD and the quenching

agent increases and the fluorescence is recovered.

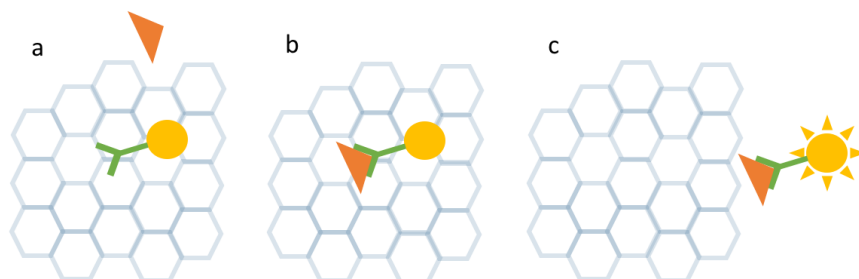


Figure 2.9: Turn-on fluorescence sensor. The yellow dot symbolized the QD, the green Y is the antibody (or other sensing agent), the red triangle is the target, e.g. the nitroaromatic explosive and the honeycomb pattern in the background symbolizes the graphene, which acts as the quenching agent. a) The QD-sensing agent complex is quenched by the graphene. b) The target molecule binds to the antibody which leads to c), an increased distance between QD and the graphene, and thereby a recovery of fluorescence.

Fluorescence quenching can be caused by several mechanisms [29]:

- dynamic quenching a.k.a. collisional quenching
- static quenching a.k.a ground-state complex formation
 - heavy atom effect
 - charge transfer
 - photo induced charge transfer
- energy transfer

In addition to true quenching mechanism, "inner filter effects", change in concentration and photobleaching can also lead to a reduction in fluorescence intensity. In an analysis, these effects have to be taken into account. Changes in concentration can be compensated for and, luckily, both the CdSe/CdS/ZnS QDs and the GQDs have negligible photobleaching.

2.5.1 Inner filter effects

The fluorescence depends on the amount of light that reaches the fluorescing agent together with the probability of photo-excitation to occur once the light has arrived. Other things in the solution, e.g. target, quencher and even the fluorescing agent itself, might scatter or absorb light on its path to the fluorescing agent. This reduces the light intensity that is available for excitation. In my experiments, the quenching agents (TNT and Dinitrotoluene (DNT)) absorb a

lot of light. To determine whether there is quenching through the above listed quenching interactions, or just a reduction of excitation light intensity that is strong enough to give an apparent quenching signal without such interactions, an inner filter correction has to be performed. The correction should take into account the actual light transmitted to the fluorescing agent, and then from the fluorescing agent to the detector.

A simple way to do so is by correcting the fluorescence based on the transmission of the solution at the excitation and emission energies [30]. This is done by using Beer-Lamberts law for transmittance as a function of absorbance:

$$T(\lambda) = 10^{-A(\lambda)} \quad (2.1)$$

where T is the transmittance and A is the absorbance at wavelength λ . The absorbance of an attenuator is defined as

$$A_i(\lambda) = \varepsilon_i \int_0^\ell c_i(z) dz \quad (2.2)$$

where ε_i is an attenuation coefficient at wavelength λ , c_i is the concentration and ℓ is the path length of the beam of light through the sample. I assume that the c_i is independent of z , and therefore get

$$A_i(\lambda) = \varepsilon_i c_i \ell \quad (2.3)$$

The path length is the parameter of interest at the moment. A simplifying assumption is that the sample is situated at a single point, in the center of the cuvette used for the PL measurements. The path length for the incident excitation intensity as well as the emission intensity is $d/2$ where d is the width of the cuvette. This is illustrated in figure 2.10.

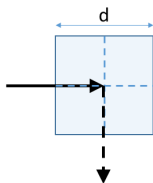


Figure 2.10: The assumed path of the excitation (horizontal) and emission (vertical) light beam through the cuvette.

When doing absorbance measurements, the beam passes through the whole cuvette. Therefore, the measured absorbance should be divided by 2 when calculating the resulting fluorescence with equation 2.1. The difference in absorption between the excitation and emission wavelength should also be considered.

The resulting correction takes the shape of

$$F_{corr}(\lambda_{ex}, \lambda_{em}) = F_0(\lambda_{ex}, \lambda_{em}) \cdot 10^{\frac{A_{ex} + A_{em}}{2}} \quad (2.4)$$

where F_0 is the measured fluorescence intensity, and F_{corr} is the resulting corrected intensity, which is larger than F_0 [30].

2.5.2 Dynamic quenching

For collisional quenching to happen, the fluorescing agent has to be in an excited state. Upon collision with the quenching agent, the fluorescing agent relaxes to its ground state non-radiatively. The quenching efficiency depends on the diffusion rate of the molecules and the probability of quenching upon collision [29]. The kinetics of collisional quenching can be described by the Stern-Volmer equation

$$\frac{F_0}{F} = 1 + k_q \tau_0 \cdot [Q] \quad (2.5)$$

where F_0 is the original fluorescence intensity, F is the intensity after quenching, k_q is a quenching rate coefficient, τ_0 is the lifetime of the excited state of the fluorescing agent and Q is the concentration of quencher. The Stern-Volmer constant is defined as $K_D = k_q \tau_0$. If there is an uncertainty as to whether or not the quenching is actually dynamic, the Stern-Volmer constant is labeled K_{SV} instead [29].

2.5.3 Static quenching

Static quenching, or ground state complex formation, is when a quenching agent forms a non-fluorescing complex with the fluorescing agent. It depends on the association constant, K_S , between quencher and fluorescing agent:

$$K_S = \frac{[FQ]}{[F][Q]} \quad (2.6)$$

Here, $[FQ]$ is the concentration of the complex, $[F]$ is the remaining concentration of the fluorescing agent and $[Q]$ is the remaining concentration of the quenching agent. The remaining fluorescence after complex formation, F/F_0 , will be the same as the fraction of the fluorescing agent that remain unquenched;

$$\frac{F}{F_0} = \frac{[F]}{[F] + [FQ]} \quad (2.7)$$

By taking the inverse of this equation, and then inserting 2.6, we get:

$$\frac{F_0}{F} = 1 + K_S \cdot [Q] \quad (2.8)$$

This expression has the same shape as equation 2.5, and it is therefore difficult to distinguish dynamic and static quenching. Difficult, but not impossible. It can be done by doing fluorescence decay measurements, as dynamic quenching should result in shorter lifetime whilst static quenching should decrease the apparent concentration of fluorescing agent. Another way to distinguish between static and dynamic quenching is by varying the temperature. An increase in temperature will increase the diffusion rate and thereby the collisional quenching, but not the static quenching. Collisional quenching doesn't affect the absorption spectra, but the formation of complexes can produce perturbations in absorption by both components, which is a third way to distinguish between these two types of quenching.

2.5.4 Modifications of the Stern-Volmer relation

Static and dynamic quenching

It is possible for there to be a combination of static and dynamic quenching. In this case, the Stern-Volmer equation has to contain two quenching constants, and takes the form

$$\frac{F_0}{F} = (1 + K_S \cdot [Q])(1 + K_D \cdot [Q]). \quad (2.9)$$

The order of $[Q]$ in this equation is two, and this will result in an upward curvature when plotting F_0/F as a function of the concentration of quenching agent. To find the individual quenching constants, equation 2.9 is rewritten by multiplication of the two terms:

$$\frac{F_0}{F} = 1 + (K_S + K_D) \cdot [Q] + K_S K_D \cdot [Q]^2. \quad (2.10)$$

By writing this expression as

$$\frac{F_0}{F} = 1 + K_{app}[Q] \quad (2.11)$$

with

$$K_{app} = \left(\frac{F_0}{F} - 1 \right) \frac{1}{[Q]} = (K_S + K_D) + K_S K_D [Q], \quad (2.12)$$

and fitting the measured quenching to K_{app} linearly, $K_S + K_D$ will be the intersection with the y-axis and $K_S K_D$ is the slope of fitted function [29].

Sphere of action

Some of the quenching mechanisms described below allow the fluorescing and quenching agent to interact over a distance. If a quencher is within a certain distance of the fluorescing agent, there will be quenching. This would yield a sphere of action around the fluorescing agent. By finding the fraction of fluorescing agents that don't have quenchers within their sphere of action, a modified Stern-Volmer relation can be obtained [29]. This is done by assuming a Poisson distribution of the quenching agents. The probability of finding k quenchers in a volume V is

$$P(k) = \frac{\lambda^k}{k!} \exp(-\lambda) \quad (2.13)$$

where λ is the mean number of quenchers in that volume. The mean number of quenchers is given by the $[C] \cdot V$. The probability that a fluorescing agent is visible is the same as the probability that there are zero quenchers within the sphere of interaction, $P(0) = \exp(-\lambda)$.

The Stern-Volmer equation thereby takes the shape

$$\frac{F_0}{F} = (1 + K_D \cdot [Q]) \cdot \exp([Q]V), \quad (2.14)$$

where V is the volume of the sphere. V can be interpreted as a static quenching constant. A sphere of action will give rise to an upward curvature in the original Stern-Volmer plot.

Multiple binding sites

Another modification to the Stern-Volmer relation arises from the possibility that there are several binding sites for the quencher on the fluorescing agent. Regarding QDs as fluorescing agents and some sort of molecule as the quencher, this is often true. A combination of multiple binding sites and dynamic quenching lead to this modification of the Stern-Volmer expression:

$$\frac{F_0}{F} = 1 + K_D[Q] + K_{MS}[Q]^n + K_D K_{MS}[Q]^{n+1}, \quad (2.15)$$

where n is the number of binding sites for the quenching agent on the QD [31]. This modification arises from a modified association constant:

$$K_{MS} = \frac{[FQ]}{[Q][F]^n} \quad (2.16)$$

which gives

$$\frac{F_0}{F} = 1 + K_{MS} \cdot [Q]^n. \quad (2.17)$$

The same derivation as for the mix of static and dynamic quenching (equation 2.9-2.12) can then be used to get the final expression. Multiple binding sites give rise to a downward tilt in the original Stern-Volmer plot.

2.5.5 Quenching mechanisms

The actual quenching mechanism behind the measured decrease in fluorescence intensity can differ between different system. Here, a closer description of different mechanisms that might be involved will follow.

Energy transfer by electron exchange

Quenching by electron exchange, illustrated in figure 2.11, consists of the excited electron (or hole) being transferred to an excited state in the quenching agent, and a non-excited electron being transferred back to the fluorescing agent [29]. The quenching agent is left in an excited state. The fluorescing and quenching agents have to be in close proximity for charge transfer to be possible. The wave functions of donor and acceptor have to overlap, otherwise the electron cannot be transferred. In other words, charge transfer requires contact at van-der-Waals radii, where the wave function is non-zero.

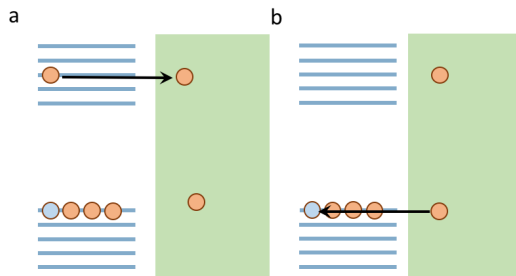


Figure 2.11: Illustration of quenching by electron exchange. The excited electron is transferred into the quenching agent, and a quenching agent is transferred to the fluorescing agent. The quenching agent is left in an excited state.

There also has to be a spectral overlap between the fluorescing agent and quenching agent, otherwise the electrons cannot be exchanged [29].

Photoinduced electron transfer

When the fluorescing agent is in its excited state, it can either accept an electron from the quencher at the unoccupied state left after the excited electron, or transfer the excited electron to the quencher. This is illustrated in figures 2.12 and 2.13.

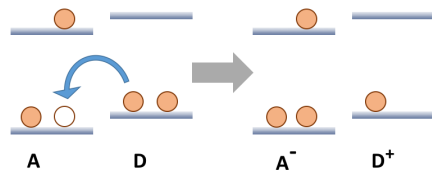


Figure 2.12: Illustration of photoinduced electron transfer, where the fluorescing agent acts as electron acceptor (A) and the quenching agent as electron donor (D). After excitation, an electron from D is transferred to the empty state in A (left). This turns A into a negatively charge ion and D into a positively charged ion.

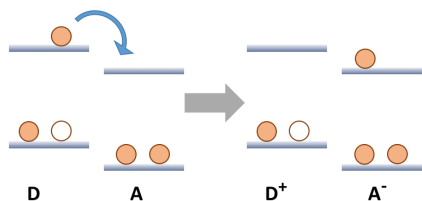


Figure 2.13: Illustration of photoinduced electron transfer where the fluorescing agent acts as electron donor (D) and the quenching agent as electron acceptor (A). After excitation, the excited electron in D is transferred to A. The result is a positively charged quenching agent and a negatively charged fluorescing agent.

The total energy of the system is decreased after the charge transfer, which is necessary for the process to take place. After the transfer, the acceptor and donor can combine again to return the transferred electron and thereby returning to the ground state by releasing the energy as heat. For photoinduced electron transfer to happen, the quenching and fluorescing agent have to be in close proximity of one another [29].

Energy transfer

The quenching phenomena mentioned above require contact between the fluorescing and quenching agent. Energy can also be transferred over a distance by a phenomena called resonance energy transfer, or more commonly Förster resonance energy transfer (FRET) [29]. In FRET, the energy is transferred

from a donor (fluorescing agent) to an acceptor (quenching agent) by a dipole interaction. The excited electron in the donor relaxes, and simultaneously an electron in the acceptor is excited. This is illustrated in figure 2.14. In the acceptor, the electron relaxes vibrationally, or by emitting light. In this project, all the quenching agents are non-emitting. For FRET to be possible, the two molecules have to be within the Förster distance, but the electron clouds do not have to overlap.

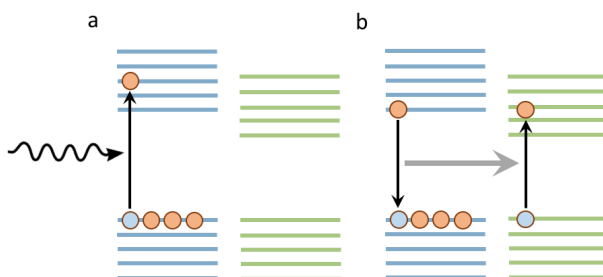


Figure 2.14: Illustration of quenching by FRET. The photon-excited electron relaxes. Simultaneously, the energy is transferred to the quenching agent by a dipole-dipole coupling, which leaves the quenching agent in an excited state.

The efficiency of FRET depends on spectral overlap between the emission of the fluorescing agent (energy donor) and the absorption of the quenching agent (energy acceptor), as well as on the distance between the two.

Nanometal surface energy transfer (NSET) is another quenching mechanism that doesn't require contact [6]. In the case of NSET, there is no dipole-dipole interaction between the quenching and fluorescing agent. Instead, it involves a dipole (fluorescing agent) and a metal surface. Persson et. al. were first in describing the formation of a dipole induced electron-hole pair at the surface of metals [32]. The consequence is a distance dependence of d^4 in NSET, to be compared to d^6 in FRET [33, 6].

The physics behind these phenomena is beyond the objective of this project. What is of interest is that they both provide quenching over a distance. FRET depends on a dipole-dipole interaction, and NSET on a dipole-metal surface interaction.

2.6 Targets for detection

2.6.1 Organic gunshot residue

As mentioned in section 1.1.2, possible targets in organic GSR are nitrocellulose, nitroglycerine and nitroguanadine. The chemical structures of these compounds

are shown in figure 2.15.

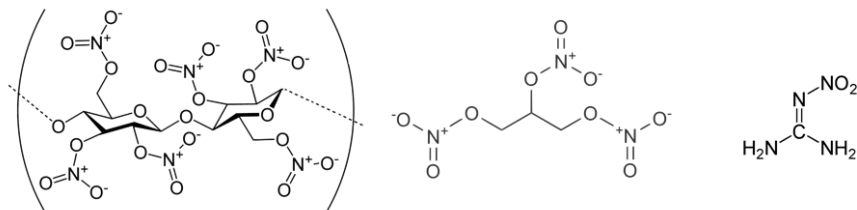


Figure 2.15: Chemical structure of nitrocellulose, nitroglycerine and nitroguanidine.

Nitrocellulose is a base component of propellant, and it would therefore be a suitable compound for identification of GSR. However, it is nitrated cellulose, which is a natural polymer. The large size of the molecular chains makes quantitative detection through fluorescence difficult. The second most common component is nitroglycerine, which is present in both double and triple base powder. Nitroguanidine is only present in triple base powder, and is thereby less suitable as an identifier of GSR. Riskin et. al. present a Molecularly imprinted polymer (MIP) based sensor for nitroglycerine [34]. It would be possible to use MIPs for sensitive detection of GSR as well as explosive compounds, but it is cumbersome and time-consuming to develop them, and not viable in a master thesis project.

Another path for detection of nitroglycerine could be by developing sensitive antibodies or aptamers. These antibodies (aptamers) could then be linked to QDs. If the QDs are quenched in the ground state, the reaction between an antibody (aptamer) and target can produce an increase in distance between QD and quencher, leading to a recovery of fluorescence. Thereby, a turn-on fluorescence detection would be achieved [35].

I have investigated the quenching of semiconductor QD fluorescence with rGO, but antibodies and aptamers are not included in this project.

2.6.2 Nitroaromatic explosives

Aromatic compounds containing nitro functional groups are common in military explosives. 2,4,6-trinitrotoluene (TNT) and 2,4-, 2,6- and 3,4-dinitrotoluene (DNT) are common nitroaromatic explosives. The chemical structures are shown in figure 2.16.

As with nitroglycerine, nitroaromatic molecules can be selectively detected with , antibodies and aptamers.

Nitroaromatic compounds also have a strong affinity for π - π -stacking on graphene. In graphene, electrons are delocalized in the sp^2 network of carbon atoms, as

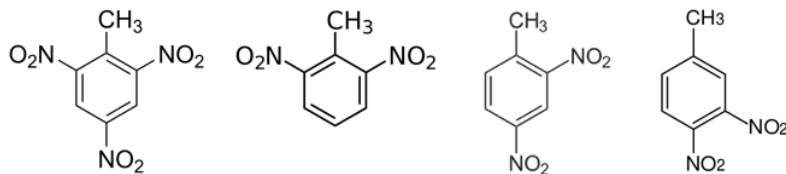


Figure 2.16: Chemical structure of 2,4,6-TNT, 2,6-DNT, 2,4-DNT and 3,4-DNT.

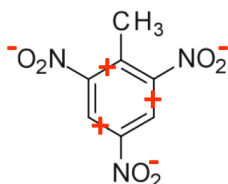


Figure 2.17: Electron withdrawing nitro groups result in electron deficiency on the aromatic ring of nitroaromatics.

shown in figure 2.3. This makes the graphene rings electron rich. The nitro groups in the nitroaromatics are electron-withdrawing, meaning that they attract the electron from nearby atoms. Therefore, there is an electron deficiency in the aromatic ring in the center of the molecules, as shown in figure 2.17. The electron deficient nitroaromatic molecules will stack on top of the graphene matrix [36, 37, 38].

Defects and functional groups on the graphene surface can further enhance the affinity, as e.g. hydroxyl groups and epoxy bridges can act as electron donors, increasing the electron concentration in the aromatic graphene rings. There might also be an electrostatic attraction between the oxygen containing functional groups on the rGO surface and the nitro groups in the nitroaromatic compounds [36].

2.7 Instruments

I have investigated fluorescence as a detection mechanism, and most of the methods used for the investigation are therefore spectroscopic. Here, a short introduction to spectroscopy will be given followed by descriptions of the specific instruments.

2.7.1 Spectroscopy

The energy of a molecule can be divided into translational energy, rotational energy, vibrational energy and electronic energy [39]. The translational energy corresponds to movements through space. The rotational energy depends on rotational movements of the molecule around its center of mass, and the vibrational energy depends on oscillatory movements between the atoms in relation to the center of mass. The electronic energy depends on the electronic density, e.g. how the electrons are distributed in the molecule. Electronic energy levels are quantized, but appear as bands because of vibrational sublevels, which are quantized and appear as bands because of rotational sublevels, which are also quantized [23]. This is illustrated in figure 2.18. The energy structure of molecules can be measured with a variety of spectroscopic methods. The methods that I have used during the project are described in the following sections.

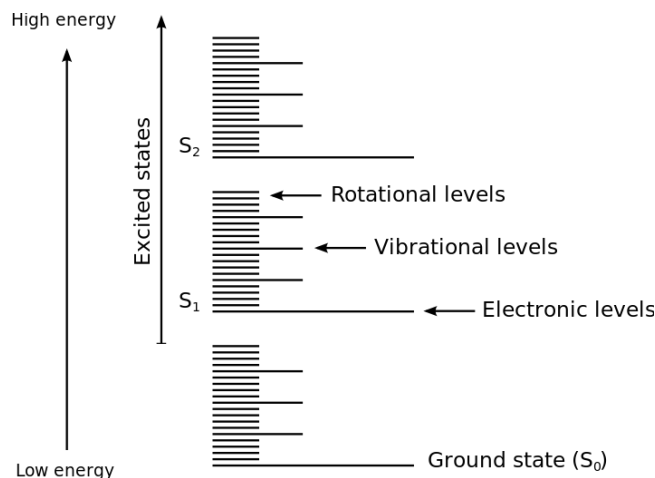


Figure 2.18: Schematic sketch of electronic energy bands consisting of vibrational and rotational sublevels. Image from © Levien van Zon, Wikimedia Commons / CC-BY-SA-3.0

Absorption of electromagnetic radiation resulting in a transition between two electronic level corresponds to the Ultraviolet-visible spectroscopy (UV-VIS) range and it is studied in UV-VIS spectroscopy. The fluorescence occurring when the electrons return to their ground state corresponds to the same energy range, and is studied in Photoluminescence (PL) spectroscopy. The vibrational transitions are of lower energies, and correspond to the IR range which is studied in Fourier transform infra-red spectroscopy (FTIR).

2.7.2 UV-VIS spectroscopy

Absorption spectroscopy in the ultra-violet and visible region gives information about electronic transitions, as the incoming light is absorbed through excitation of electrons from a lower to a higher molecular orbital. Excitation will happen if the energy of the incident light matches the energy difference between two electronic energy levels. The absorption bands in the UV-VIS range are broadened by vibrational and rotational sub-bands [23].

The possible electron transitions are [23]:

$\sigma \rightarrow \sigma^*$: This is a high energy transition because σ -bonds are strong. Normally, these transitions cannot be seen in UV-VIS because the corresponding wavelength is below 200 nm, and thereby too short for regular UV-VIS spectroscopy.

$n \rightarrow \sigma^*$: The transition from a non-bonding state to a anti-bonding σ -state. Although the energy is lower than that of the $\sigma \rightarrow \sigma^*$ transition, it is still quite high, often out of range for UV-VIS measurements. The non-bonded electrons are difficult to excite if the molecule is polar. There has to be a non-bonded electron for this transition to occur.

$\pi \rightarrow \pi^*$: The excitation of an electron from a bonding to a non-bonding π -orbital can happen in all compounds that contain a π -bond, e.g. C=C and C=O.

$n \rightarrow \pi^*$: This is the transition that requires the lowest energy, and it is usually the strongest.

In graphene, the energy of the $\pi \rightarrow \pi^*$ transition in the C=C bond is ~ 270 nm. In GO, the same $\pi \rightarrow \pi^*$ transition is at ~ 230 nm and a second peak from $n \rightarrow \pi^*$ transitions in C=O appears at ~ 300 nm [21]. Because of the difference in transition energy, UV-VIS can be used for monitoring the reduction process of rGO.

For GQDs, the $\pi \rightarrow \pi^*$ in C=C peak appears between 200 and 270 nm, and the second C=O $n \rightarrow \pi^*$ transition lands above 260 nm [40].

Figure 2.19 shows a simplified setup for UV-VIS measurements. A monochromator is used for tuning the wavelength. The light beam passes through the sample and a reference containing the solvent. The absorbance of the reference is subtracted from the sample absorbance.

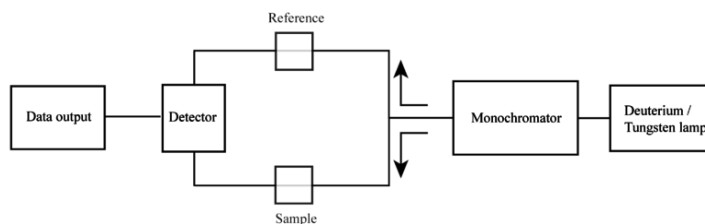


Figure 2.19: Simplified sketch of a UV-VIS setup from [41].

2.7.3 Photoluminescence Spectroscopy

The wavelengths studied in PL spectroscopy correspond to electronic transitions in atoms/molecules. Compared to UV-VIS spectroscopy, where the absorption of light is used to gain information about the molecular structure, PL concerns the de-excitation of the excited electrons, in other words the emission of light.

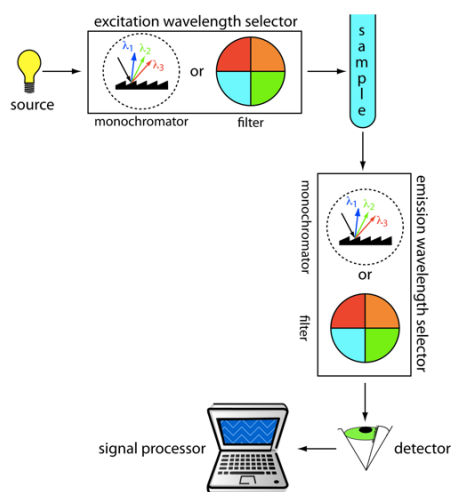


Figure 2.20: Schematic sketch of Image from ©David Harvey (DePauw University)/ CC-BY-SA-3.0 [42]

When doing a PL measurement, a specific wavelength is chosen as the excitation wavelength. A detector placed in an angle from the light source then scans over a specified range, and a spectrum is obtained. This spectrum shows the emission of light at different wavelengths induced by excitation at one specific wavelength. A simple sketch of a typical PL setup is shown in figure 2.20. The first monochromator chooses a wavelength from the light source, and the second monochromator is used for detecting the fluorescence intensity at different wavelengths.

The physics of monochromators result in second order harmonic peaks (e.g. if exc. is at 325 nm, there will be a second order harmonic peak at 650 nm). These peaks originate from both monochromators. Firstly, the excitation monochromator will let a small amount of light of the double wavelength pass through. Secondly, if there is strong scattering in the sample, second order peaks will occur as some of the 325 nm light will be detected when the second monochromator is set to 650 nm [29].

Photoluminescence excitation (PLE) measurements consist of selecting an emission wavelength and then scanning the excitation wavelength. It is useful for determining the most efficient excitation wavelength if the emission wavelength is known.

2.7.4 FTIR

In FTIR spectroscopy, IR absorption is studied. Infrared radiation in the NIR/MIR range is absorbed by the vibrational states in the molecules, giving a change in vibrational energy. Infrared Radiation from $400\text{-}4000\text{ cm}^{-1}$ is useful for determining composition of organic compounds [43].

The energy spectra of the vibrational-rotational bands depend on the strength of the bond between the two vibrating atoms and the masses of the two atoms, the neighboring atoms and the geometry of the molecule. Vibrations are usually categorized as stretching or bending and can be both symmetrical and asymmetrical. The molecular vibrations can cause a rhythmic change in the dipole moment of the molecule, which is the same as a change in the electric field. Only the dipole-changing vibrations can be seen in FTIR, as the change in electric field from the vibration couples with the electric field of the IR radiation [23, 44].

Although it is possible to calculate the energies of specific bonds theoretically, it is very cumbersome. Therefore, tables with the wavenumber of characteristic functional groups as well as conjugations, and reference data, is used for analysis of FTIR spectra.

The absorption of a sample for a specific wavelength can be measured by shining monochromatic light through the sample. FTIR is more time efficient, as a Michelson interferometer is used for creating a range of interference patterns and measuring the absorption for each pattern. The Michelson interferometer splits the light into two paths, and the length of one of the paths is varied using a set of mirrors. This produces an interference. As the mirrors are moved, data is produced in the time domain. Fourier transformation converts the data to the frequency domain [44].

When interpreting an FTIR spectra, the frequency of the absorption peaks as well as their strength is evaluated. The strength of a peak depends on two things: repetition and polarity. The more bonds of a specific type, and the

more polar a molecule is, the stronger the peak. The peaks can be very very small, e.g. if the polarity of the bond is very small, but still contain valuable information.

Conjugation, which means that there are alternated single and double bonds in a molecule, lowers the energy of the whole molecule. This means that the frequency in the FTIR spectrum is lowered as well. Therefore, a peak originating from a bond can vary slightly in wavenumber, depending on adjacent functional groups.

2.7.5 SEM-EDS

In SEM-EDS, the SEM part stands for Scanning Electron Microscopy, and involves a high energy electron beam being focused on the sample. The directly back-scattered electrons together with second order electrons emitted by the sample are collected by a detector, and the data is used to create an image of the sample [45].

The electron bombardment results in emission of X-rays from the sample. When secondary electrons are produced from inner electron shells in the atoms, a hole is left at that energy level. The hole is filled with an electron from a higher energy level, and the transition results in emission of an X-ray photon. Since every element has its own unique atomic energy structure, the X-ray contains information about the elemental compositions of the sample. In EDS, these X-rays are collected and analyzed [45].

3 Methods and Materials

3.1 GSR sampling

GSR samples were collected at a shooting range in Stockholm. SEM-EDS analysis was performed successfully. Attempts were made to use other analytical methods to determine organic components, e.g. FTIR, but no successful results were achieved.

The conventional collection method for GSR samples consists of using adhesive carbon film to collect the particles. This is suitable for analysis in SEM-EDS because the carbon films are suitable substrates for SEM, and the collection stubs can therefore be analyzed directly, without further preparation. However, for analysis of organic components, adhesive carbon stubs might contaminate the samples. Therefore, I used swabs consisting of 1/4 of a cotton pad, dampened with Isopropanol, as this had previously been described as an efficient method for collection [46].

Samples were taken from the floor, the shooter and directly from the gun. The floor samples were taken 1.5 and 2 m in front of the shooting dock, with a dry and a damp cotton swab, respectively, and from the wall next to the shooter. Gun samples were taken by swabbing the chamber and the pipe with dampened cotton cloths. The hand samples were swabbed from the right and left hand of the shooter. The person performing the sampling was wearing clean gloves and the shooter washed his/hers hands before shooting, all to avoid contamination. A reference hand sample was collected just before shooting.

The challenge was to separate the GSR components from the cotton swabs. First, ultrasonication of the swabs didn't yield any results. Second, centrifugation (8000 rpm, 10 min) was tried. This resulted in some precipitation of GSR particles. These were placed on Si-substrates for further analysis. SEM was used to pick out particles that looked like GSR, and EDS was performed on those particles. The investigated samples were from inside the pipe of the gun, from the floor in front of the shooting bench and from the hand of the shooter.

3.2 Synthesis and characterization of rGO

In this project, I reduced the GO with AA, as described in section 2.3. Several batches were produced to optimize the results. Details of the rGO synthesis are given in appendix A.

The resulting rGO was analyzed with UV-VIS, PL and FTIR and the results are shown in section 4.2. From the results, the level of reduction of the GO is discussed. For the UV-VIS and PL characterization, the rGO had to be diluted to a suitable concentration to avoid saturation. Sample preparation for FTIR measurements consisted of dropcasting diluted rGO on double polished Si (for transmission measurements) or on gold substrates (for reflectance measurements).

3.3 QD fluorescence quenching with rGO

Quenched semiconductor QDs is the ground state for turn-on fluorescence detection. To investigate this type of sensor, I started out with measuring the quenching efficiency of rGO by mixing rGO with fluorescing QDs, and comparing the fluorescence intensity before and after addition of rGO.

A small amount of QDs was diluted with water, so that the fluorescence intensity was suitable for the PL instrument. Thereafter, rGO was added to the solution and the mix was stirred. Changes in fluorescence were monitored with PL spectroscopy.

Both excitation and emission slit was set to 10 mm during the measurements.

3.4 Synthesis and characterization of GQDs

GQDs were prepared according to the recipe in Appendix 2, inspired by [28] as discussed in section 2.4. In short, glucose and water was mixed and placed in a glass bottle with a plastic, Teflon-lined lid. Kapton tape was applied around the lid to further improve the pressure holding capability of the bottle. The MAH heating was applied with varied time and intensity.

To investigate the composition of the synthesized GQDs, the obtained samples were characterized with PL and UV-VIS after dilution to suitable concentrations. The GQDs were also drop-casted on gold substrates and examined with FTIR. The results are shown in section 4.5.

3.5 GQD fluorescence quenching by nitroaromatic compounds

As described in section 2.6, nitroaromatic explosives have a high affinity for π - π -stacking on graphene lattice. The consequential quenching of the GQD fluorescence was measured with PL. The GQDs were diluted to suitable concentration for the PL measurement. Thereafter, TNT and DNT reference solutions were added, and the changes in both PL and UV-VIS absorption was monitored. The UV-VIS measurements are necessary for inner-filtering corrections, as described in section 2.5.1. The results are shown in 4.6. In these measurements, both excitation and emission slit of the PL was set to 10 mm. The nitroaromatics used in the experiments were calibration samples purchased at AccuStandard. 2,4,6-TNT, 2,4-DNT and 2,6-DNT were dissolved in acetonitrile (figure 3.1) and methanol. 3,4-DNT was dissolved in methanol. The concentration of explosives in the samples was 1 mg/ml.

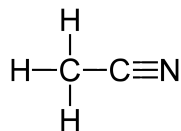


Figure 3.1: Chemical structure of acetonitrile.

3.6 Turn-on fluorescence by addition of nitroaromatics to graphene-quenched semiconductor QDs

The last experiment consisted of adding nitroaromatic explosives to the already quenched semiconductor QDs. The concept is described in section 1.2.

Here, the aim was to almost completely quench the QDs, and then monitor the change in fluorescence upon addition of nitroaromatics. The same procedure as in section 3.3 was used for the quenching of the QDs. Thereafter, nitroaromatics were added to the solution.

It is difficult to reach the right level of quenching without adding excess rGO, but an attempt was made. In the results, section 4.7, no turn-on signal can be detected. There is a further decrease in fluorescence when the nitroaromatics are added.

4 Results and discussion

4.1 SEM-EDS of gunshot residue

The conventional method for detection of GSR is SEM-EDS. First, the sample is scanned using SEM to identify particles that could originate from the combustion in the chamber. This is followed by EDS analysis of the identified particles which gives a composition spectra. Some results of SEM-EDS performed on the samples obtained from the shooting range are shown in the figures below.

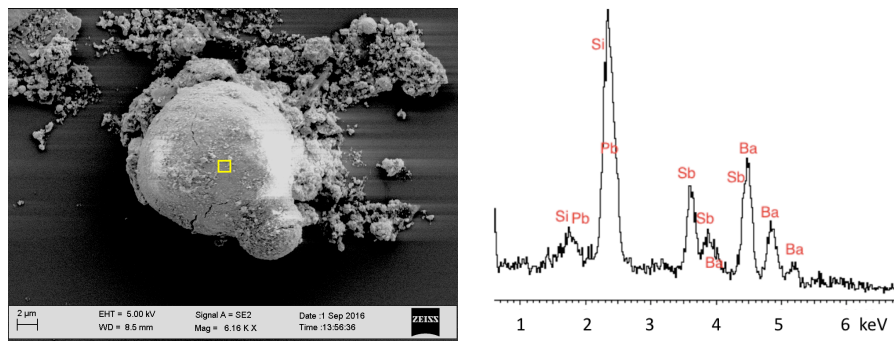


Figure 4.1: GSR particle from the pipe of gun. Left: SEM of the particle. Right: EDS of the area marked in the figure to the left.

Most of the spectra showed the unique GSR combination of Pb-Ba-Sb, as in figure 4.1. Figure 4.2 and 4.3 shows the EDS spectra of the sample obtained from the floor of the shooting range. In the left EDS spectra of figure 4.3, left, no clear Sb peak could be identified. This might be because that specific particle, i.e. the ammunition that the particle originates from, did not contain any Antimony. Under forensic circumstances, this result would not be valid as proof for GSR.

On the same particle, a second spectra was taken from one of the brighter bumps (area marked as B in figure 4.2). The spectra can be seen in to the right in figure

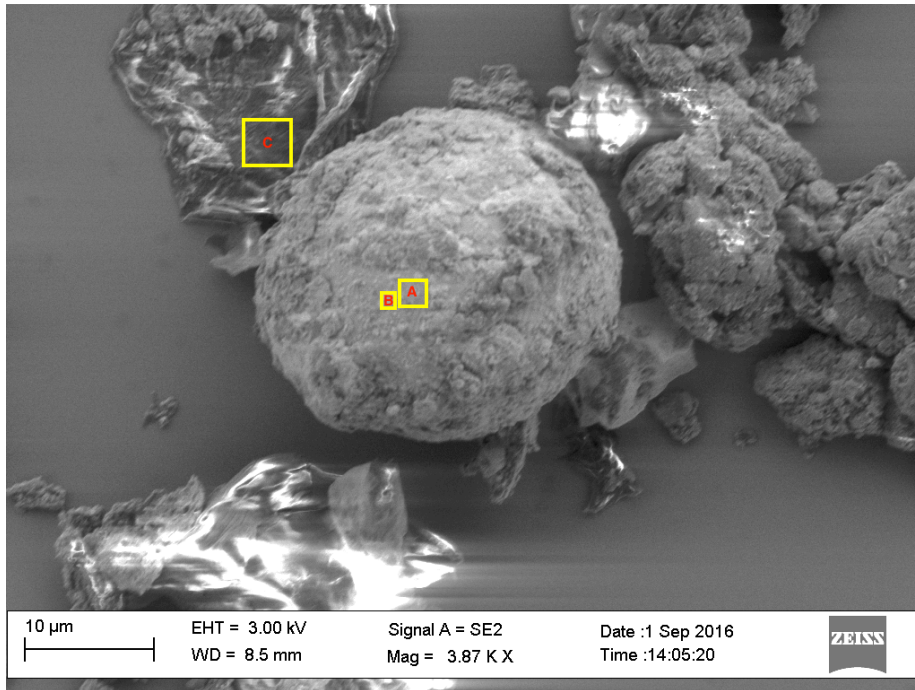


Figure 4.2: GSR particle from the floor in front of shooting bench at underground shooting range. The areas where EDS was performed are marked.

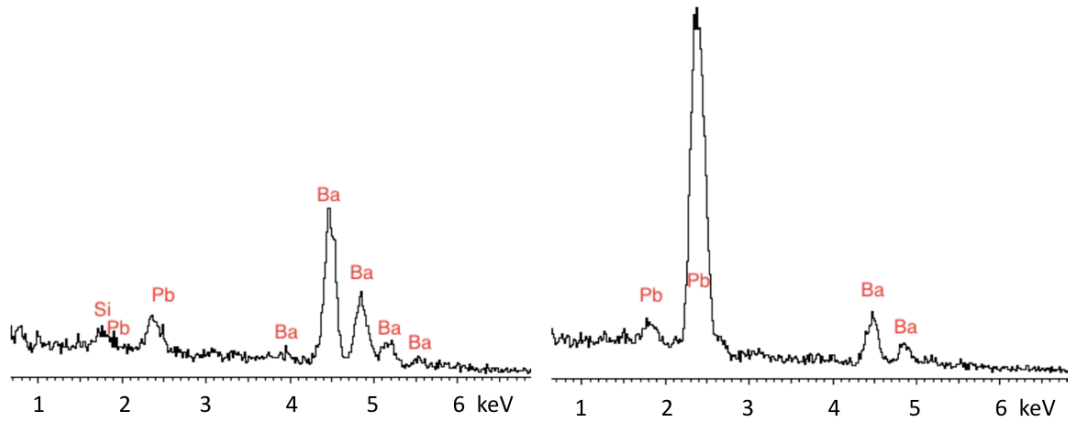


Figure 4.3: EDS spectra of area A and B in figure 4.2.

4.3 and shows a high peak for lead. Lead has a higher atomic number (82), and therefore backscatters electrons more strongly compared to e.g. Barium (56),

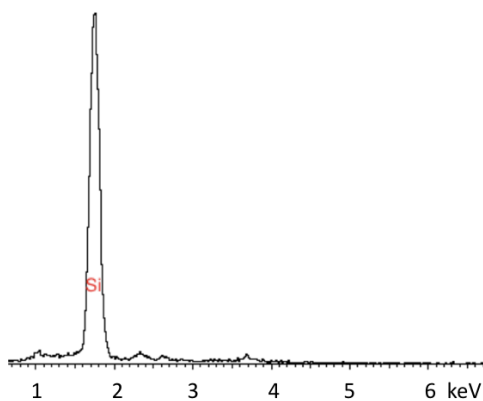


Figure 4.4: EDS spectra of area C in figure 4.2.

which explains the difference in brightness. The explanation for why there are zones with higher lead-content might be found in the combustion process and particle formation process, but is outside the scope of this project.

The last spectra, figure 4.4, is taken from the dirt next to the GSR particle, the zone marked "c" in figure 4.2. The only peak originates from Si. The substrates used were made of Silicon, so that peak is likely to originate from the substrate. The spectra also shows small peaks from oxygen and carbon. Although these peaks should not be taken too seriously, as many substances have similar spectra, they might indicate that the dirt is organic. Both the dirt on the floor as well as not fully combusted propellant etc from the gun contain organic substances.

4.2 Characterization of rGO

The results from the reduction process with ammonia and ascorbic acid will be presented here. The progress of the reduction was monitored by UV-VIS absorbance spectroscopy, as shown in figure 4.5. For GO, there are two absorbance peaks at 230 nm and 300 nm corresponding to a π - π^* -transition and a $n - \pi^*$ transition, respectively. The transitions are further described in the theory section 2.7.2. During reduction, the $n - \pi^*$ peak at 300 nm decreases since it originates from an O-C bond and oxygen is removed in the reduction process. A graphene π - π^* peak appears at 270 nm for fully reduced graphene. It appears as if the π - π^* transition peak blue-shifts through the reduction process, starting at 230 nm (GO) and finishing at 270 nm (rGO). In fact, for partially reduced rGO, the apparent peak somewhere between 230 and 270 nm is a mix of the GO and rGO peaks. As the reduction proceeds, the intensity of the rGO peak increases and takes over completely for fully reduced rGO.

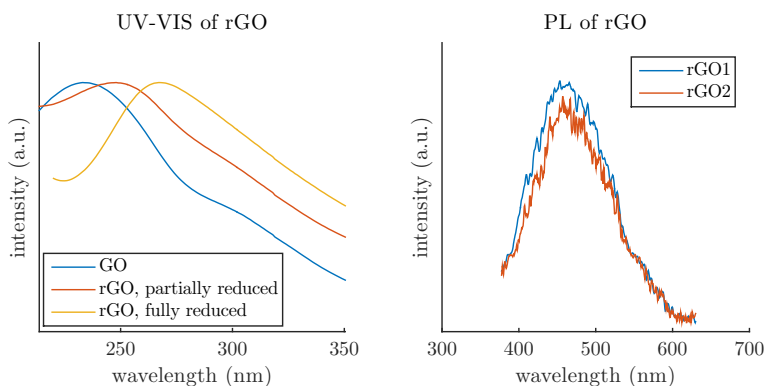


Figure 4.5: UVVIS spectroscopy of GO and partially and fully reduced rGO. PL of rGO.

Chemically derived graphene, including rGO, usually shows some PL around 450-500 nm. This is due to surface states from functional groups and lattice defects [47]. The rGO that I have synthesized has the same behavior, which is shown in the right plot in figure 4.5. Luckily, the intensity is low enough not to have any significance in the tests performed later on.

Figure 4.6 shows the FTIR-spectra of GO and rGO.

The broad peak above 3000 cm^{-1} corresponds to O-H-stretching. The large and broad OH-peak in the rGO spectrum indicates that the reduction is incomplete. This is common for rGO as some oxygen containing functional groups remain after the reduction. This peak in the GO spectrum is unreasonably small. I don't know why that is.

The double peak at $2930\text{-}2950 \text{ cm}^{-1}$ corresponds to sp^3 C-H stretch, and the

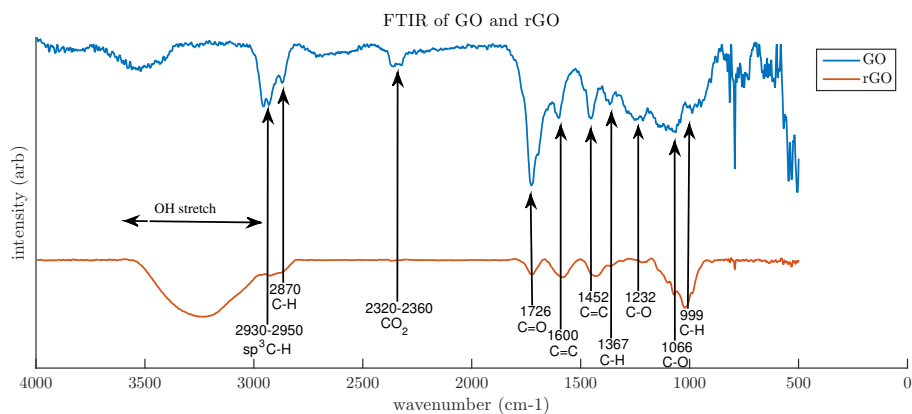


Figure 4.6: FTIR of GO and rGO.

peak at **2870 cm^{-1}** probably corresponds to aldehyde C-H stretch (that is, a conjugated C-H stretch due to a double-bonded oxygen on the C). The decrease in amplitude of these peaks for rGO compared to GO indicates a regain in graphene structure.

The double peak at **2320-2360 cm^{-1}** corresponds to C=O stretch. This peak is usually prescribed to carbon dioxide. However, these measurements were done in vacuum and the peak might therefore correspond to C=O bonds in GO. If that is the case, there is a clear reduction of C=O bonds in the rGO.

The region around **1726 cm^{-1}** corresponds to C=O stretches. Depending on neighboring structure, e.g. if it is a carbonyl, carboxylic, ester, aldehyde or ketone C=O, the exact energy may vary. The peak is a lot larger in GO compared to rGO, which supports that a reduction has occurred. Since there is a small remaining peak in the rGO, the reduction is incomplete.

The peaks at **1600 cm^{-1} and 1452 cm^{-1}** correspond to C=C stretch in aromatic rings, and might demonstrate a recovery of the graphene aromatic rings, especially when comparing the amplitude of these peaks and the sp^3 peaks around 2900 cm^{-1} .

The small peak at **1367 cm^{-1}** probably corresponds to sp^3 C-H bends, and these are more common on GO, since it lacks in the graphene-typical sp^2 -hybridization when comparing it to rGO.

The small peak at **1232 cm^{-1}** probably corresponds to a C-O bond.

The peak at **1066 cm^{-1}** corresponds to another C-O bond, and this one seems almost completely depleted in the rGO.

Finally, the peak at **999 cm^{-1}** originates from sp^2 C-H bends.

Although it is hard to interpret FTIR spectra quantitatively, there are several

differences in the obtained data that indicate that there has been some reduction of the GO.

In summary, the characterization results correspond well with literature. The rGO can be considered well reduced due to the shift in UV-VIS absorbance wavelength. This doesn't mean that all oxygen containing functional groups were removed - there are still surface and edge groups as well as defects in the graphene lattice, which is confirmed by the FTIR. The FTIR results are more difficult to interpret, but several of the differences between the two spectra indicate that there has been some reduction of the GO.

4.3 Semiconductor QD characterization

The results of the characterization measurements done on the core-shell semiconductor QDs from Prof. Ying Fu (Science For Life Laboratory at KTH) will be presented here. The QDs consist of CdSe/CdS/ZnS and are capped in 3-MPA (see figure 2.6). Figure 4.7 shows the FTIR spectra of the QDs and of pure 3-MPA. The the QDs don't absorb energy in the IR range. However, the 3-MPA coating (figure 2.6) contains several functional groups, and should therefore show up in FTIR.

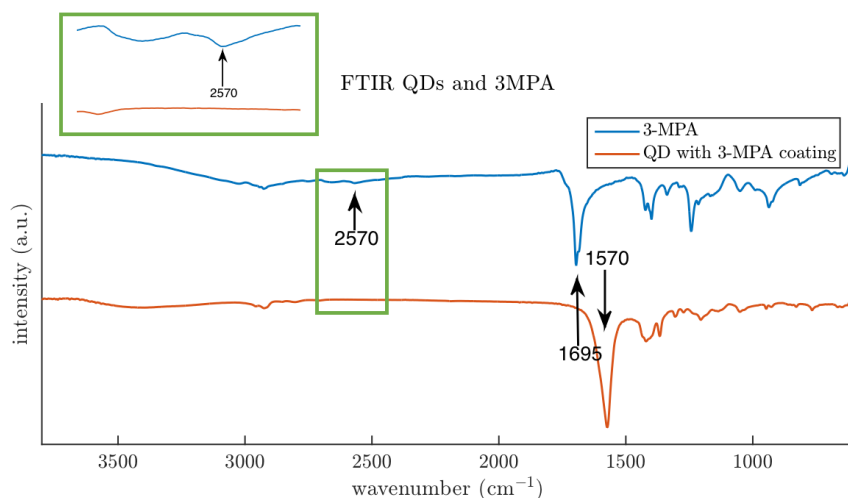


Figure 4.7: FTIR of CdSe-CdS/ZnS QDs and 3-MPA.

The spectra are very similar, except for a shift in the absorbance peak around 1700 cm⁻¹, and a small S-H peak around 2570 cm⁻¹. The S-H peak, which only exists in the pure 3-MPA, confirms that the 3-MPA binds to the QDs through the thiol group. Assuming that the large peaks originate from the C=O bond,

Ke et. al. state that a “spacial distortion resulting from a high density ligand layer”, leading to a shift to lower wave numbers for the bonded 3-MPA, can occur [48]. It can therefore be concluded that the 3-MPA coating is of high density.

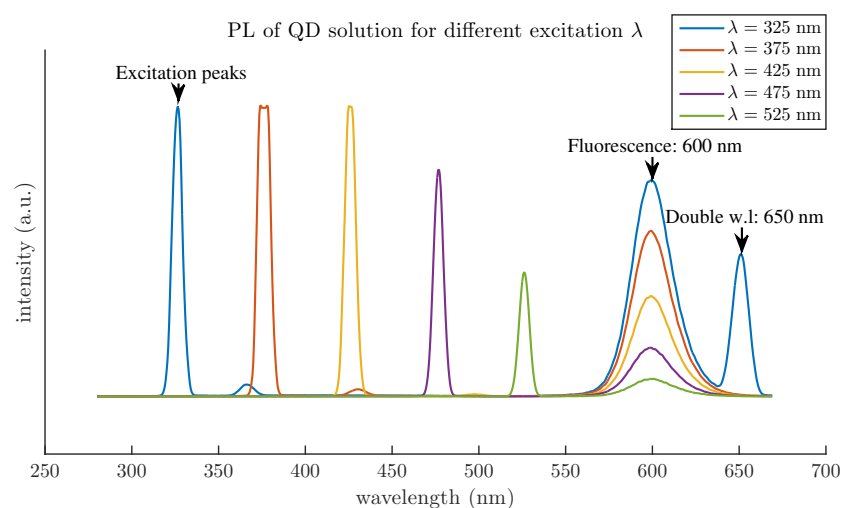


Figure 4.8: PL of QDs for different excitation wavelength. Both excitation and emission slits were set to 7 mm.

The PL spectra of the QDs was examined to determine suitable parameters for future quenching measurements. Figure 4.8 shows PL spectra for manually varied excitation wavelength. The fluorescence peak is strongest for excitation at 325 nm, and this excitation wavelength was therefore used for the quenching experiments. Attention should be given to harmonics of the excitation and emission wavelength to avoid misinterpretation of the results.

4.4 Quenching of semiconductor QD fluorescence with rGO

In this section, the quenching efficiency of rGO on the fluorescence of semiconductor QDs is examined. Figure 4.9 (left) shows the fluorescence intensities for large amounts of rGO. To the right, the relative maximum intensity is plotted as a function of the rGO concentration. F_0 is the maximum intensity without quencher and F is the intensity after addition of quenching agent. The plot shows saturation for high concentrations of rGO.

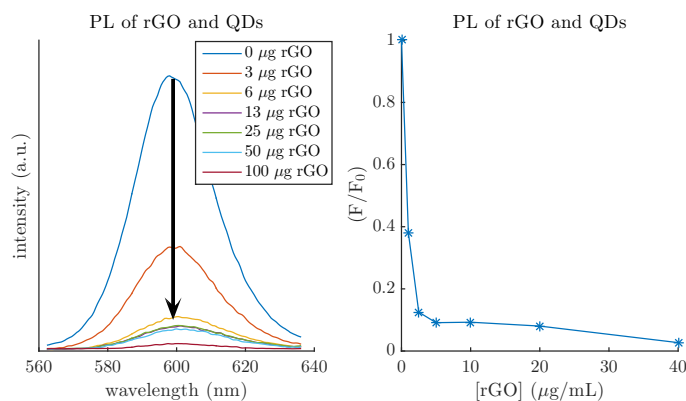


Figure 4.9: Quenching of CdSe/CdS/ZnS QD fluorescence by rGO. Left: Fluorescence intensity for different amounts of rGO. The arrow shows the quenching direction. Right: Relative intensity as a function of concentration of rGO.

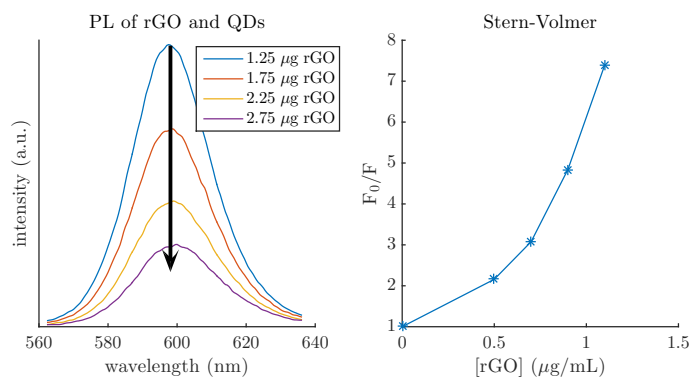


Figure 4.10: Quenching of CdSe/CdS/ZnS QD fluorescence by rGO. Left: Fluorescence intensity for different concentrations of rGO. The arrow shows the quenching direction. Right: Stern-Volmer plot of the fluorescence quenching.

Figure 4.10 (left) shows the fluorescence intensity for lower concentrations of rGO. The right plot in figure 4.10 shows the inverse relative intensity as a

function of the concentration of rGO. This is called a Stern-Volmer plot. It is the conventional way of plotting quenching and can be used to quantify the quenching and deduce the quenching mechanism. Before further analysis of the Stern-Volmer plot, I want to consider the different quenching mechanisms that might be present.

According to many references, rGO quenches QD fluorescence via FRET or NSET [6, 20, 33, 49]. For FRET, there has to be a spectral overlap between the emission of the fluorescing agent (the QDs) and absorbance of the quenching agent (the rGO). At a first glance, it seems like there is no spectral overlap between rGO and QDs in figure 4.11, as the peaks are far apart. But although the wavelength of the absorbance peak of rGO doesn't coincide with the emission peak of the QDs, there *is* absorbance at the QD emission wavelength. Because of this spectral overlap, FRET is a possible quenching mechanism. NSET can happen even if there is no spectral overlap, as long as the dipole of the fluorescing agent couples with a metal surface (see section 2.5.5). Graphene isn't a metal, but it has many metal-like properties and NSET is therefore possible [49].

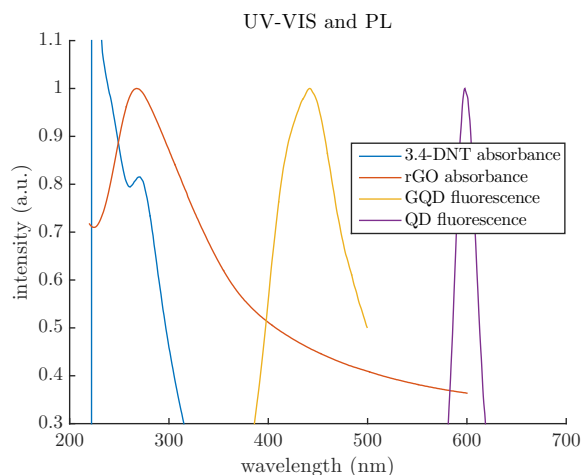


Figure 4.11: Absorbance of 3,4-DNT and rGO and emission of GQDs and semiconductor QDs.

For electron exchange and photoinduced electron transfer, the QDs and rGO have to be in close contact. Even though the QDs might adsorb on the rGO (which is probably the case), the 3-MPA coating of the core-shell QDs passivates the outer surface of the QDs. This means that the excited electron is unlikely to leave the core of the QD. So even though the substances are in close proximity, the quenching still has to occur over a distance. This supports FRET or NSET at quenching mechanism.

Regarding the adsorption of QDs on the rGO surface: the oxygen containing end groups (-COOH) of the 3-MPA capping are likely to bond electrostatically

with the remaining oxygen-containing groups on the rGO, which will place the substances close to each other. Since there is a bond between the fluorescing and quenching agent, the quenching should be static.

Now is a good point to return to the Stern-Volmer plot in figure 4.10. The upward curvature is a deviation from the typically linear relationship which might indicate that there is both dynamic and static quenching, in accordance with equation 2.9. A second explanation is that diffusion equilibrium hasn't been reached yet, but that the quenching is static. This would add a diffusion dependent term, just as the dynamic term in equation 2.9.

A third explanation is that there is no static quenching, but that the quenching occurs without the particles being in contact. Assuming that there is a sphere of action around the fluorescing agent, and that the quenching will happen if the quenching agent is within this sphere, the quenching efficiency increases as shown in equation 2.14.

I have already concluded that the quenching is most likely happen through the FRET or NSET mechanism, and that is is probably static due to electrostatic bonding between the QDs and rGO. Since the quenching is static, no diffusion dependence should be present. However, I still attempted to modify the Stern-Volmer plot for each of the scenarios above. These results are shown in figure 4.12.

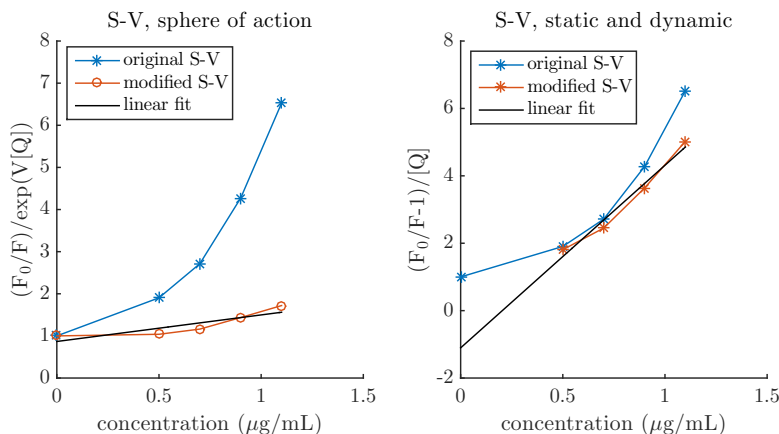


Figure 4.12: Modified Stern-Volmer plots for a sphere of interaction (left) and a mix of static and dynamic quenching (right).

These modifications didn't yield very good results. In the first case, the modified curve is still far from linear. However, a K_{sphere} value of 630 mL/ μ g can be deduced. In the second case, the modified curve intersects with the y-axis at a negative value. This will result in a negative Stern-Volmer coefficient, which wouldn't make any sense as there is a clear quenching of fluorescence.

To check whether or not the solution is in diffusion equilibrium, the time-

dependence of the quenching is plotted in figure 4.13. It shows an increase in quenching over time, as the intensity goes down to 91 % of the original intensity after 10 minutes. Although the increase is small, no saturation can be deduced from figure 4.13, and as some of the measurements took around 10 minutes, this could have an effect on the results. The decrease in fluorescence could be due to an increase in the number of QDs adsorbed on the rGO over time. Another explanation is that the QDs and QD-rGO complexes sediment, which would also lead to a reduction in fluorescence intensity. Either way, this effect is too small to explain the full curvature of the Stern-Volmer plot.

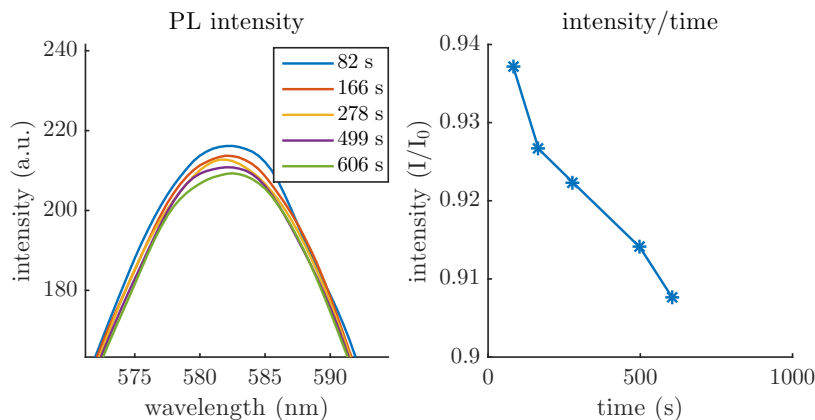


Figure 4.13: Time dependence of fluorescence intensity after addition of quencher.

In summary, it can be concluded that rGO is an efficient quencher of QD fluorescence. It is possible that the QDs adsorb electrostatically on the rGO surface. From that, it would follow that the quenching is static. Although the actual quenching mechanism cannot be deduced from these results, nothing indicates that the previously reported FRET or NSET is incorrect.

One possible explanation for the deviations from the expected linear Stern-Volmer relation is that the concentration of rGO is too high. From figure 4.9, it is clear that the quenching saturates for high concentrations for rGO. Although the concentrations used in the Stern-Volmer analysis were considered low at the time of the experiment, there might still be errors originating from saturation. Another error source is that the results have not been corrected for the inner-filtering effect, and this might affect the results. However, a lack of inner-filter correction should result in a downward curvature rather than an upward curvature, and the absorbance of TNT of rGO at the current concentrations is very very small.

The possible adsorption of the QDs on the rGO is good for quenching, but not as good for sensing applications. For the sensing mechanism described in figure 2.9), the antibody or aptamer based turn-on fluorescence sensor to work, the recovery of fluorescence should depend on the target molecules. If the QDs are

attracted to the graphene, they might remain in close proximity when the target molecule is added. This means that no signal would be achieved. The problem can be solved with another type of surface coating, one that doesn't bond with the graphene.

4.5 Graphene quantum dot characterization

GQDs were synthesized by the MAH process described in section 3.4. Figure 4.14 shows the UV-VIS absorbance, PLE and PL spectra of the obtained particles. For reference, the absorbance spectra of glucose is also included as the GQDs were synthesized from glucose.

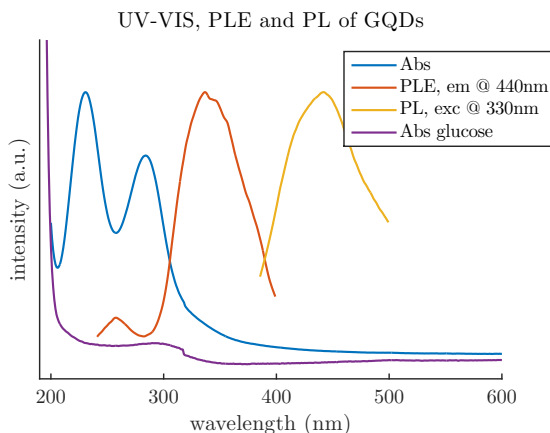


Figure 4.14: UV-VIS absorbance, PLE and PL spectrum for GQDs and UV-VIS of glucose for reference.

I will start with discussing the absorbance peaks, which are situated at 231 and 284 nm for the GQDs. Glucose has a low absorbance peak around 300 nm and another at 450 nm. In reference to the absorbance values of GO and rGO, as shown in section 4.2 (230 and 300 nm for GO and 270 nm for rGO), the absorbance peaks are closer to those of GO compared to rGO. The peaks coincide well with the expected values for GQDs as mentioned in section 2.7.2. Specifically, the peak at 231 nm is most likely to originate from a π - π^* transition, and the peak at 284 nm indicates functional groups and/or defects giving one or more non-bonding energy levels somewhere between the π and π^* levels.

Moving on to the PLE and PL spectra, there are two GQD PLE peaks (emission at 440 nm) at 258 and 337 nm, and there is a fluorescence peak at 442 nm for excitation at 330 nm. Glucose has no visible fluorescence peak, and thus no detectable PLE peaks. The fact that the solution is fluorescent after the synthesis process shows that *something* has happened, but from the data in

figure 4.14, little can be said about the amount of graphene structure in the GQDs. To determine whether or not the synthesized fluorescent particles have graphene lattice, the FTIR spectra is studied.

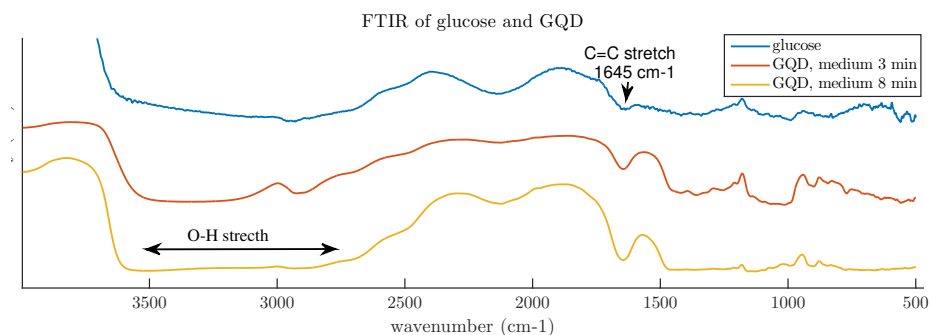


Figure 4.15: FTIR of glucose and GQD. The GQDs were synthesized at medium intensity for 4 and 8 minutes.

Figure 4.15 shows the FTIR spectra of glucose and GQDs. There is an increase in the sp^2 C=C bond at 1645 cm^{-1} in the synthesized dots compared to the glucose. This might indicate an increase in graphene lattice.

When studying the PL of the GQDs for different excitation wavelengths, figure 4.16, it is clear that the luminescence is excitation dependent. For longer excitation wavelengths, a second peak at 493 nm becomes visible. For shorter excitation wavelengths, there are two shoulder peaks at 390 nm and 415 nm.

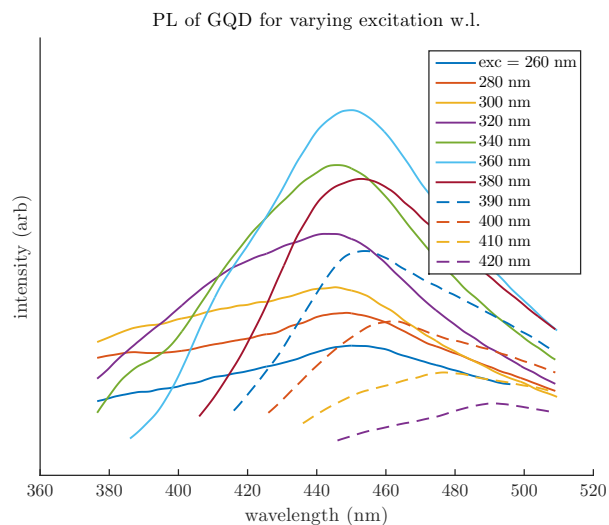


Figure 4.16: PL intensity of GQDs for varying excitation wavelength.

One explanation for the excitation dependent emission is based on emissive traps originating from the surface states. With excitation at a specific wavelength, a trap corresponding to a specific type of defect or functional group is activated, and will dominate the emission.

In figure 4.17, I present a possible energy structure for the GQDs based on the emissive trap theory and the transitions that can be identified in the UV-VIS absorbance and PL spectra. The transitions are linked to the π - π^* -transitions as well as intermediate states.

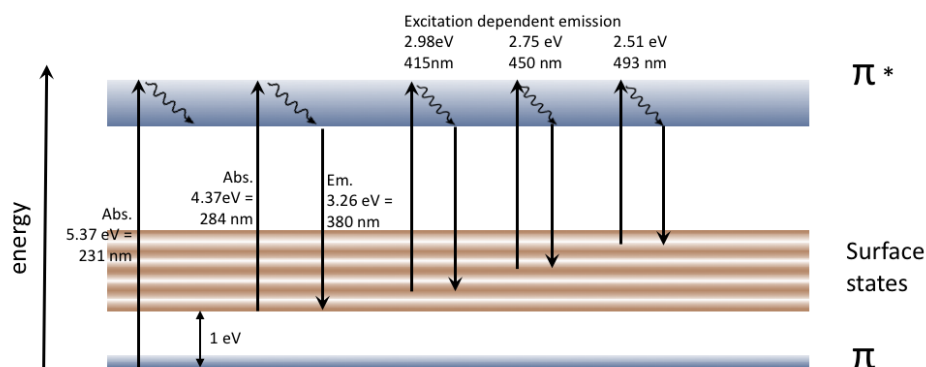


Figure 4.17: Proposed energy structure with emissive surface traps, adaption from [28].

No PL has been measured for the π - π^* -transition, because the excitation wavelength is too short for the PL setup. Therefore, no emission arrow has been drawn for that transition.

The two PLE peaks in figure 4.14 should also be related to electronic transitions, but I have not managed to fit them into the structure of figure 4.17.

The excitation dependent PL measurements could also be explained with some sort of optical selection depending on the size of the GQDs [50]. In simple terms: maybe a specific wavelength is more likely to be absorbed by particles of a specific size. If the PL is size dependent, this would lead to excitation dependent emission. However, no size dependent PL characteristics was noted by [28] and therefore, the surface state emissive trap model is more likely.

In an attempt to optimize the synthesis process and investigate potential differences in properties depending on the synthesis time, I varied the microwave heating time and studied the samples with PL. The results can be seen in figure 4.18 where the intensity is displayed for different heating times, and in figure 4.19, where the maximum intensity (left) and wavelength maximum (right) is plotted as a function of time.

There seems to be an increase in intensity for increasing MAH heating time,

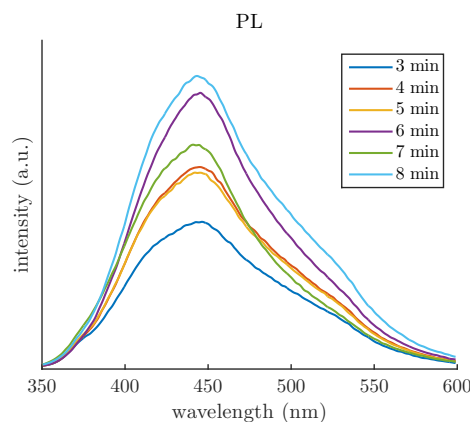


Figure 4.18: PL of GQD for varying microwave heating time at medium intensity.

but further studies would be needed to verify the results. Regarding tuning of wavelength, it is impossible to make out a trend from the results. The setup for the MAH synthesis could have been a lot more reliable and therefore these results should be treated with caution.

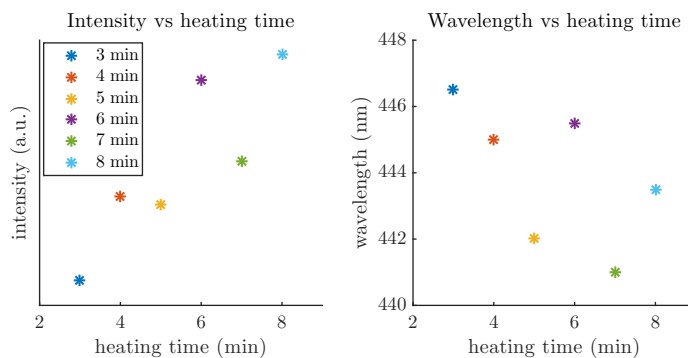


Figure 4.19: Maximum PL intensity and maximum wavelength of GQDs for varying heating time.

In summary, the GQDs characterization showed a conversion from non-luminescent glucose to a luminescent solution after the MAH synthesis. Whether or not synthesized particles are actually of graphene structure is difficult to determine from these results, but the FTIR shows an increase in C=C bonds that might originate from the sp^2 lattice of graphene, and UV-VIS absorbance measurements show similarities with GO as well as correspondence with the referenced results of Pan et al. [40]. Further investigation of the effect of changes in heating time and intensity should be done before drawing a conclusion on the optimal method, preferably with an improved heating setup.

4.6 Quenching of GQD fluorescence with nitroaromatic compounds

Before examining the quenching of GQD fluorescence by nitroaromatic compounds, the UV-VIS spectra of the analytes and their solvents were studied (figure 4.20). The solvents, acetonitrile and methanol, show practically no absorbance at the excitation wavelength. The TNT sample, however, shows a noticeable absorbance. This has to be taken into account when studying the decrease in fluorescence of the GQDs, as some of the decrease may be due to inner filter effects.

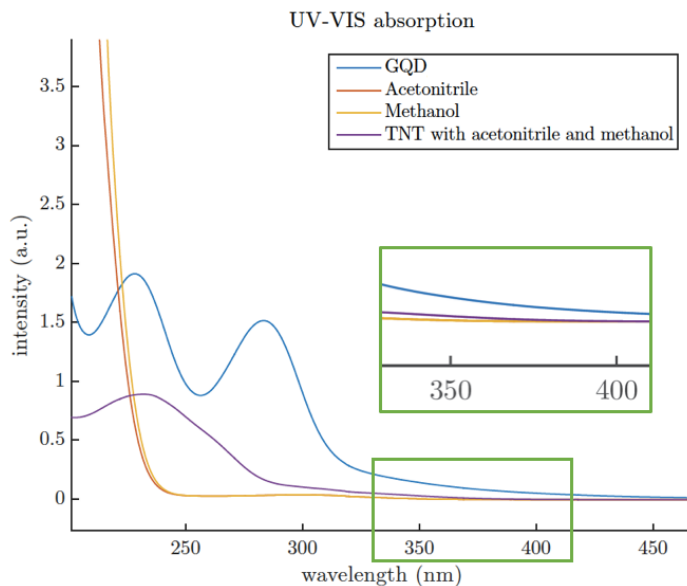


Figure 4.20: UV-VIS absorption of GQDs, TNT and solvents of the TNT sample. The TNT concentration shown on the figure is the *lowest* concentration used in the quenching experiments.

Figure 4.21 shows the fluorescence intensity of the GQDs after addition of different amounts of nitroaromatics. In figure 4.22 this data is corrected for inner filtering effects by the method described in section 2.5.1. This decreases the apparent quenching efficiency, but there is still a notable decrease in fluorescence after the correction for absorbance.

In both figures, the quenching is noticeably stronger for the 3,4-DNT. Theoretically and according to literature [51] TNT should be a better quencher, as it contains more functional groups and should therefore bond more strongly to the graphene (see figure 2.16). The functional groups enhance the π - π -stacking affinity of nitroaromatic molecules on rGO, and might also affect the quenching

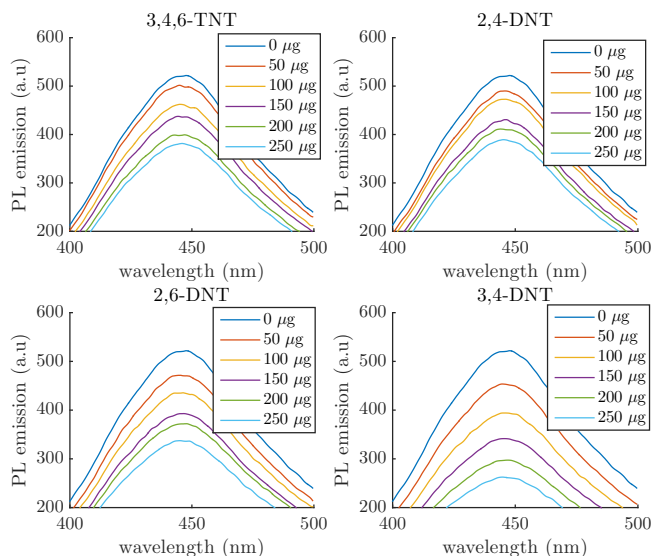


Figure 4.21: PL for varying amount of nitroaromatics. Excitation at 360 nm.

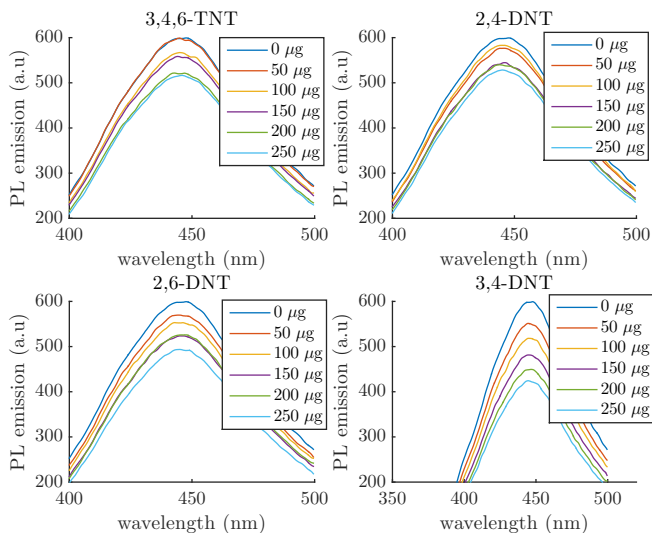


Figure 4.22: Inner filter corrected PL intensity.

efficiency, which will be discussed below.

The explanation for the difference in quenching efficiency can be found in the solvents of the explosive samples: The nitroaromatics used in this experiment were dissolved in a mix of methanol and acetonitrile, except for the 3,4-DNT which was dissolved in pure methanol. They were (unfortunately) provided like

this from the manufacturer. The acetonitrile passivates the nitroaromatics by reducing the electronegativity of the functional groups. The 3,4-DNT solution doesn't contain acetonitrile, which means that the functional groups are active. It is probable that the quenching would have been stronger for TNT without acetonitrile. But two active functional groups are better than three passivated functional groups, and 3,4-DNT is therefore the most efficient quencher among the nitroaromatics that I tested.

The first graph in figure 4.23 shows the effect of the inner filter correction. The original maximum intensity as a function of nitroaromatic concentration is plotted with dashed lines and the corrected data is plotted with stars. The apparent quenching efficiency is decreased. The second graph is a Stern-Volmer plot of the corrected data. It is linear, which is expected since the nitroaromatics are assumed to bond to the GQDs through π - π -stacking, which should result in static quenching.

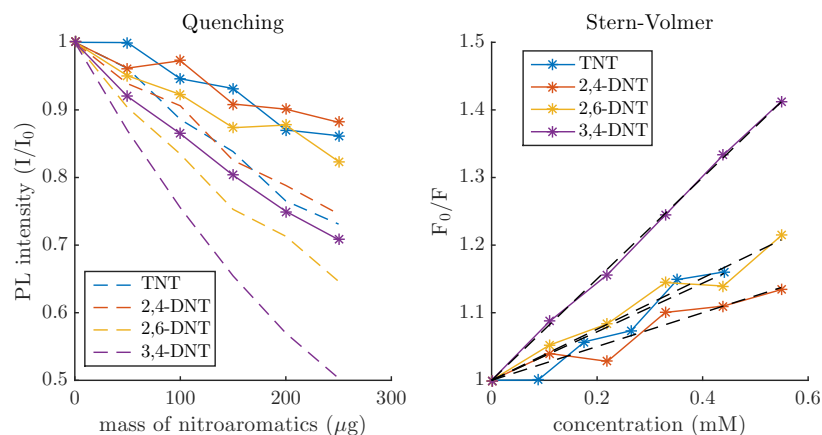


Figure 4.23: Inner filter corrected quenching of GQD fluorescence by TNT and DNT. The first plot shows the quenching before (dashed lines) and after (stars) correction for the inner filtering effect. The second figure is a Stern-Volmer plot of the corrected data, and a linear approximation of the 3,4-DNT quenching (black dashed line).

Before further analysis of the Stern-Volmer plot, I want to discuss the quenching mechanisms. I will focus on 3,4 DNT, since that is the only non-passivated target compound. To determine the quenching mechanism, the spectral overlaps of the components, figure 4.11, was studied. FRET and electron exchange require a spectral overlap between the fluorescing and quenching agent, in this case the PL of the GQDs and the absorbance of the nitroaromatics. Since there is no overlap, these FRET and electron exchange can be scratched from the list of possible quenching mechanisms. Nitroaromatics are not metals, and there are no surface properties similar to metals. Therefore, NSET can be excluded.

Photoinduced electron transfer is still a possible quenching mechanism: the

nitroaromatic molecules stack on the GQDs and the electron clouds are thereby close. There might also be bonding interaction between the functional groups on the GQD surface and the nitro groups on the nitroaromatic molecule, opening another path for electron transfer. The energy of the largest PL peak, 450 nm, was connected to surface states in section 4.5. This supports the hypothesis that the quenching occurs between these surface functional groups and nitro groups of the explosives. To sum it up, the quenching mechanisms involves transfer of charge and is made possible by the affinity for π - π -stacking between nitroaromatics and GQDs. The details of the transfer are undetermined.

Now, returning to the Stern-Volmer plot in figure 4.23, I will try to quantify the quenching. The Stern-Volmer constant for 3,4-DNT is calculated to 750 M^{-1} . Fan et. al. [52] report $K_{SV} = 8000 M^{-1}$ for TNT, which is 10 times as high as my value. They do not report a value for DNT, but the quenching efficiency for DNT should be lower than TNT. For the rest of the nitroaromatics, $K_{SV}(TNT) = 360 M^{-1}$, $K_{SV}(2,4-DNT) = 240 M^{-1}$, $K_{SV}(2,6-DNT) = 380 M^{-1}$. However, the error in of these results is too high to draw any real conclusions.

In summary, nitroaromatics quench the fluorescence of GQDs, and the quenching efficiency is correlated to the nitro groups since the passivation of these groups decreases the quenching. The quenching is static, and I propose charge transfer aided by the stacking of the nitroaromatics on the GQDs as the quenching mechanism. The Stern-Volmer quenching coefficient that I achieved is 750 M^{-1} for 3,4-DNT, which is 10 times lower than reported values for TNT [52].

4.7 Detection of nitroaromatics with a hybrid of semiconductor QDs and rGO

In section 1.2 and 3.6, I describe how the addition of nitroaromatics to a mix of semiconductor QDs and rGO might produce a turn-on fluorescence signal. However, there was no increase in intensity when DNT was added to a mix of rGO and QDs. Instead, the fluorescence decreased further when the nitroaromatics were added.

Figure 4.24 shows the decrease in PL for QDs and rGO+QDs when 3,4-DNT is added. The figure to the left shows the quenching of QD fluorescence by 3,4-DNT, the middle figure shows the quenching of the QD-rGO hybrid. The figure to the right shows the quenching by 2,6-DNT on QD fluorescence, which can be compared to the quenching by 3,4-DNT in the figure to the left. The quenching by 2,6-DNT is lower, which means that the acetonitrile doesn't only affect the π - π -stacking affinity on graphene structure, but also the quenching ability on semiconductor QDs. The quenching of QD fluorescence by 3,4-DNT, the figure to the left and in the middle, is very similar regardless of the content of rGO.

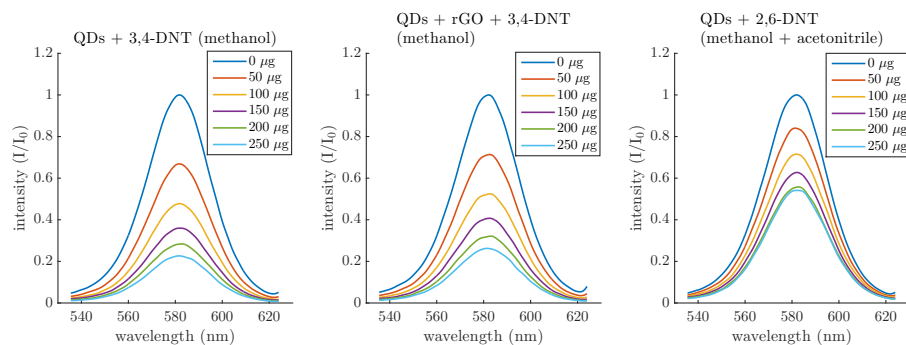


Figure 4.24: PL for 3,4-DNT in methanol, 3,4-DNT and rGO hybrid and 2,6-DNT in methanol and acetonitrile.

In figure 4.25, I compare the quenching by 3,4-DNT on semiconductor QDs, a hybrid of rGO and QDs, and GQDs. The left plot shows the relative quenching as a function of the concentration of 3,4-DNT, before and after correction for the inner filtering effect. A Stern-Volmer plot for the corrected intensities is shown in the right figure.

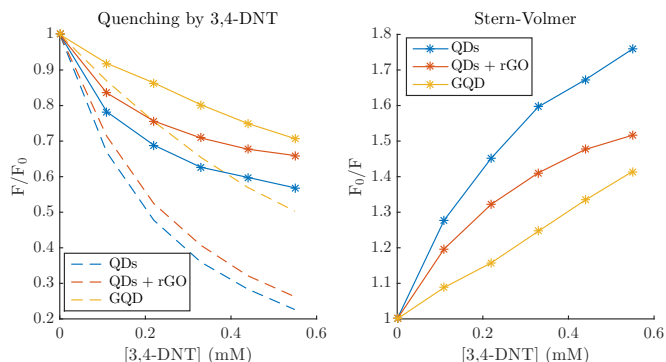


Figure 4.25: Quenching by 3,4-DNT in methanol. Semiconductor QDs, rGO-QD hybrid and GQDs as fluorescing agent. The figure to the left shows the quenching before (dashed lines) and after (stars) correcting for the inner filtering effect. The figure to the right is a Stern-Volmer plot of the inner filter corrected fluorescence.

The quenching of GQD fluorescence by 3,4-DNT has been evaluated in the section above. Here, I will focus on the quenching mechanism of DNT on the fluorescence of QDs and rGO-QD hybrid.

There is no spectral overlap between the nitroaromatics and the QDs, (figure 4.11), which means that FRET and regular charge transfer can be ruled out. NSET is not possible either, since it is based on a metal (or metal-like in the case of graphene) surface and the nitroaromatics lack this characteristic.

Photoinduced charge transfer is the possible quenching mechanism. The bonding between the coating and the nitroaromatics brings the nitroaromatic close to the surface of the QD, facilitating the photoinduced charge transfer. The bonding could also leads to a reduction in the passivating effect of the coating, which makes it possible for the QD to be relaxed by surface states instead of fluorescence. In future experiments, QDs with another type of coating less likely to react with the nitroaromatics, could be tested to further investigate the quenching.

There is a downward curvature in the Stern-Volmer plot in figure 4.25 for the QDs and the QD-rGO-hybrid. This is a deviation from the typically linear relation. It can be assigned to multiple binding sites on the fluorescing QDs. I made an attempt to fit the measured data to the modification of the Stern-Volmer relation for multiple binding sites (equation 2.15). This is shown in figure 4.26.

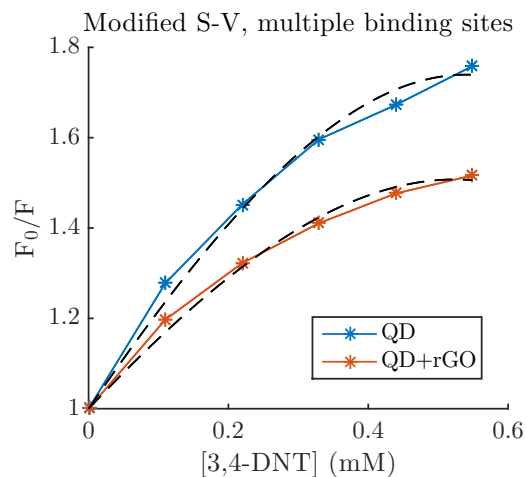


Figure 4.26: Stern-Volmer plots with data fit according to the model of multiple binding sites accordingly with equation 2.15.

Although the curve fits look better, I doubt the obtained parameters: For the QDs, K_S gets a negative value of -430 M^{-1} and $K_D = 2120 \text{ M}^{-1}$, which doesn't make sense. For the rGO-QD hybrid, $K_S = 2250 \text{ M}^{-1}$ and K_D is assigned a negative value of -630 M^{-1} . The binding site coefficients were 0.82 and 1.11 for QDs and rGO-QDs, respectively.

I tried another model for multiple binding sites, but only static quenching instead of both static and dynamic, accordingly with equation 2.17. The fit looked similar to the one in figure 4.26. Now, K_S values of 1100 and 750 M^{-1} and binding site values of 0.590 and 0.570 for QDs and rGO-QDs, respectively, was calculated. These binding site values are low compared to similar systems in literature ([31]). The residual norm was also higher compared to the fit taking both static and dynamic quenching into account, but the Stern-Volmer constants were positive, which was an improvement.

Neither of the two models for multiple bindings sites give a very satisfactory result. This might be because there aren't actually multiple binding sites, but it is more likely that the measured data contains errors, or that the inner filter correction isn't accurate enough. It is probable that there are multiple binding sites on the QDs for the nitroaromatics, as the QDs are quite large compared to the nitroaromatic molecules, and the outward -OH group on the capping agent, 3-MPA, is likely to bond electrostatically with the nitro groups on the nitroaromatics, since the former is strongly electron donating and the latter is strongly electron withdrawing.

In summary, the nitroaromatic explosives quench the fluorescence of QDs. There are probably multiple binding sites on the QDs, which gives a downward curvature in the Stern-Volmer plot. The proposed quenching mechanism is through

photoinduced charge transfer. But the nitroaromatic compounds could also react with the coating of the QDs, which would open up surface states for relaxation and thereby reduce the fluorescence.

5 Conclusion and outlook

5.1 Summary and conclusion

The aim of this project was to investigate graphene, QD and fluorescence based sensors for forensic applications. I started by doing a literature study of forensics, mainly focusing on gunshot residue and explosives. Thereafter, I investigated different how to achieve selectivity when using fluorescing semiconductor quantum dots. There are many ways, e.g. by using aptamers, antibodies or molecularly imprinted polymers. However, the time frame for investigating many of these methods was too long a master thesis project.

I chose three detection methods for further investigation. In short, the first one consisted of investigating the quenching of semiconductor QD fluorescence with rGO (functionalization of the QDs was left for the future). The second method involved GQDs, which were quenched by nitroaromatic compounds. The third one was testing if semiconductor QD fluorescence could be turned on by adding nitroaromatics to a quenched QD-graphene hybrid.

5.1.1 rGO and quenching of semiconductor QD fluorescence

To test the quenching of semiconductor QD fluorescence by rGO, I had to synthesize rGO. This was done by reducing GO with ammonia and ascorbic acid. It is a simple and green way to produce rGO, and my results coincided well with literature. Attention should be drawn to the fact that some remaining oxygen containing functional groups are inevitable.

The rGO proved to be an efficient fluorescence quencher. But the remaining functional group might be a problem for future detector systems. If they bond to the QDs there is a risk that the recovery of fluorescence upon addition of the target molecules does not happen. This can be avoided by changing the coating of the QDs.

The quenching by rGO increases over time, which reduces the usability in fast,

highly sensitive detection. But the increase in quenching is quite small (3 percentage points in 10 minutes), and the large fraction of quenching is immediate.

5.1.2 GQDs and detection of nitroaromatics

For the second experiment, I had to manufacture GQDs. Although the synthesis method had been published [28], it was less established than the one for rGO. The characterization of the produced GQDs indicated some level of graphene, but I worry that calling them graphene quantum dots is a bit of an exaggeration. Carbon dots, or carbon nanoparticles, might be a more suitable term. Further investigation is needed for a definite conclusion on the graphene properties of the particles.

My results show that nitroaromatic compounds quench GQD fluorescence. However, I couldn't prove any selectivity towards TNT, as reported in literature [51, 52]. This is because of the passivating agent in the TNT and DNT reference solutions. The same experiments with non-passivated nitroaromatics would be necessary to determine selectivity.

The DNT sample without the passivating agent clearly quenched the fluorescence. Although non-passivated TNT might be an even better quencher, the quenching by DNT means that there is a risk for false-yes results, which is very undesirable in forensic applications. Therefore, I would advise against using GQDs for selective detection of TNT. However, GQDs could still substitute the toxic semiconductor QDs that are used today.

5.1.3 Semiconductor QDs-rGO hybrids and detection of nitroaromatics

In the last experiment, I tried adding nitroaromatics to a solution of semiconductor QDs and rGO with the hope of measuring a recovery of fluorescence. But the nitroaromatics proved to quench the QD fluorescence, most likely by bonding to the 3-MPA coating. This could be avoided by changing the QD coating, but it is still improbable that the small nitroaromatic molecules can *kick out* the QDs if they are adsorbed on graphene.

In general, if turn-on fluorescence is the goal, attention should be paid to avoid direct quenching of fluorescence by the target molecule.

5.2 Outlook

There are many areas in this project that can be further investigated. Using antibodies or aptamers for fluorescence based selective detection of forensics related compounds is interesting. Specifically, an investigation of the influence of the remaining functional groups on the quenching efficiency would be interesting to investigate. This could be done by testing the quenching ability for different grades of reduction, and maybe comparing it to pristine graphene.

Regarding the affinity for π - π stacking of nitroaromatics on graphene, molecular modelling could give further information on the selectivity. Recently, the use of graphene for cyclic voltametry based detection of TNT has been reported by Yew et. al. [36]. They report higher sensitivity and selectivity, compared to what has been achieved with fluorescence based sensors. In my opinion, this would be a very interesting method for detection of TNT. A disadvantage is that cyclic voltametry can be very environment sensitive, and many of the applications in the forensic field are "dirty".

The QDs were synthesized by microwaving glucose and water in a pressurized container for 4-7 minutes. It is a very simple method. Further investigation of the characteristics of the particles would be of interest, e.g. a proper analysis of the effect of synthesis time and microwave power. Also, TEM or AFM of the QDs would give information about the particle size and shape, and further FTIR and Raman investigation could clarify the graphene properties of the particles. It would be great if QDs could substitute regular semiconductor QDs, since these are toxic.

In general, fluorescence decay measurements of all the quenching experiments would be necessary to further investigate and hopefully determine the quenching mechanisms. By measuring fluorescence decay, the dynamic quenching constant can be determined.

In the beginning, I had a vision of a little paper slip coated in functionalized QDs, that would start shining in different colors when in contact with e.g. explosives. I have let go of this vision. Although QDs are bright, the fluorescence is not that intense. Therefore, even if a similar sensor might be possible, it would lack in sensitivity. There is still a possibility of building a detector that can measure a change in intensity (with a lot higher sensitivity compared to the human eye), and thus still use a fluorescence signal for the detection. But then, the simplicity of just using a paper would be gone. If electronics are to be included, I believe that there are other means of detection that are more sensitive, e.g. cyclic voltametry as used by Yew et al. [36].

Bibliography

- [1] NFC National Forensic Center. NFC website. URL <https://nfc.polisen.se/kriminalteknik/>.
- [2] Wikipedia. Forensic science, Wikipedia, the free encyclopedia, 2016. URL https://en.wikipedia.org/wiki/Forensic_science. [Online; accessed 25-10-2016].
- [3] Z. Qian, X. Shan, L. Chai, J. Ma, J. Chen, and H. Feng. DNA nanosensor based on biocompatible graphene quantum dots and carbon nanotubes. *Biosens Bioelectron*, 60, 2014. doi: 10.1016/j.bios.2014.04.006.
- [4] C. Zhang and L.W. Johnson. Single quantum-dot-based aptameric nanosensor for cocaine. *Analytical chemistry*, 2009. ISSN 0003-2700. doi: 10.1021/ac802737b.
- [5] R.G. Smith, N. D’Souza, and S. Nicklin. A review of biosensors and biologically-inspired systems for explosives detection. *Analyst*, 2008.
- [6] M Li, X. Zhou, S. Guo, and N. Wu. Detection of lead (II) with a “turn-on” fluorescent biosensor based on energy transfer from CdSe/ZnS quantum dots to graphene oxide. *Biosensors and Bioelectronics*, 2013. ISSN 0956-5663. doi: 10.1016/j.bios.2012.11.039.
- [7] K.H. Chang, P.T. Jayaprakash, and C.H. Yew. Gunshot residue analysis and its evidential values: a review. *Australian Journal of Forensic Sciences*, 2013. ISSN 0045-0618. doi: 10.1080/00450618.2012.691546.
- [8] O. Dalby, D. Butler, and J.W. Birkett. Analysis of gunshot residue and associated materials—a review. *Journal of forensic sciences*, 2010. ISSN 1556-4029. doi: 10.1111/j.1556-4029.2010.01370.x.
- [9] F.S. Romolo and P. Margot. Identification of gunshot residue: a critical review. *Forensic Science International*, 2001.
- [10] J. S. Caygill, F. Davis, and S. P.J. Higson. Current trends in explosive detection techniques. *Talanta*, 88, 2012. doi: 10.1016/j.talanta.2011.11.043.
- [11] X. Sun, Y. Wang, and Y. Lei. Fluorescence based explosive detection:

- from mechanisms to sensory materials. *Chem. Soc. Rev.*, 44, 2015. doi: 10.1039/C5CS00496A.
- [12] F. Chu, G. Tsiminis, N. A. Spooner, and T. M. Monro. Explosives detection by fluorescence quenching of conjugated polymers in suspended core optical fibers. *Sensors and Actuators B: Chemical*, 199, 2014. ISSN 0925-4005. doi: 10.1016/j.snb.2014.03.031.
- [13] E. M. Thurman I. Ferrer. *Liquid Chromatography Time-of-Flight Mass Spectrometry*. John Wiley & Sons, Inc., 2008. ISBN 9780470429969.
- [14] A.K. Geim and K.S. Novoselov. The rise of graphene. *Nat Mater*, 6(3), 2007. doi: 10.1038/nmat1849.
- [15] K.S. Novoselov, V.I. Falko, L. Colombo, P.R. Gellert, M.G. Schwab, and K. Kim. A roadmap for graphene. *Nature*, 490(7419), 2012. doi: 10.1038/nature11458.
- [16] C. Marinelli A. Zurutuza. Challenges and opportunities in graphene commercialization. *Nat Nanotechnology*, 9(9), 2014. doi: 10.1038/mnano.2014.225.
- [17] C. Chua and M. Pumera. Chemical reduction of graphene oxide: a synthetic chemistry viewpoint. *Chemical Society Reviews*, 43(1), 2013. doi: 10.1039/C3CS60303B.
- [18] W. Ren and H.M. Cheng. The global growth of graphene. *Nature Nanotechnology*, 9(10), 2014. doi: 10.1038/nnano.2014.229.
- [19] D. Vasudevan, R.R. Gaddam, Trinchi A., and Cole I. Core-shell quantum dots: Properties and applications. *Journal of Alloys and Compounds*, 636, 2015. doi: 10.1016/j.jallcom.2015.02.102.
- [20] H. Liu, G. Fang, H. Zhu, C. Li, C. Liu, and S. Wang. A novel ionic liquid stabilized molecularly imprinted optosensing material based on quantum dots and graphene oxide for specific recognition of vitamin E. *Biosensors and Bioelectronics*, 47, 2013. doi: 10.1016/j.bios.2013.03.006.
- [21] L. Li, G. Wu, G. Yang, J. Peng, J. Zhao, and J.J. Zhu. Focusing on luminescent graphene quantum dots: current status and future perspectives. *Nanoscale*, 2013.
- [22] *Principles of Organic Chemistry*. Elsevier, Boston, 2015. ISBN 978-0-12-802444-7. doi: 10.1016/B978-0-12-802444-7.00001-X.
- [23] L.D.S. Yadav. *Organic Spectroscopy*. Springer Science+Business Media Dordrecht, 2005. ISBN 978-94-017-2508-8.
- [24] K. S. Novoselov, A. K. Geim, S. V. Morozov, D. Jiang, Y. Zhang, S. V. Dubonos, I. V. Grigorieva, and A. A. Firsov. Electric field effect in atomically thin carbon films. *Science*, 306, 2004. doi: 10.1126/science.1102896.

- [25] W.S. Hummers and R.E. Offeman. Preparation of graphitic oxide. *Journal of the American Chemical Society*, 80(6), 1958. doi: 10.1021/ja01539a017.
- [26] M.J. Fernández-Merino,, L. Guardia, J.I. Paredes, S. Villar-Rodil,, P. Solís-Fernández,, A Martínez-Alonso,, and J.M.D. Tascón. Vitamin c is an ideal substitute for hydrazine in the reduction of graphene oxide suspensions. *J Phys Chem C*, 114(14), 2010. doi: 10.1021/jp100603h.
- [27] J. Zhang, H. Yang, G. Shen, P. Cheng, and J. Zhang. Reduction of graphene oxide via l-ascorbic acid. *Chem. Commun.*, 2010. doi: 10.1039/B917705A.
- [28] L. Tang, R. Ji, X. Cao, J. Lin, H. Jiang, X. Li, K. Teng, C. Luk, S. Zeng, J. Hao, and S. Lau. Deep ultraviolet photoluminescence of Water-Soluble Self-Passivated graphene quantum dots. *ACS Nano*, 6(6), 2012. doi: 10.1021/nn300760g.
- [29] J. R. Lakowicz. *Principles of Fluorescence Spectroscopy*. Springer, 2010.
- [30] X. Luciani, S. Mounier, R. Redon, and A. Bois. A simple correction method of inner filter effects affecting FEEM and its application to the PARAFAC decomposition. *Chemometrics and Intelligent Laboratory Systems*, 96(2), 2009. doi: 10.1016/j.chemolab.2009.02.008.
- [31] W. Chen, X. Wang, X. Tu, D. Pei, Y. Zhao, and X. Guo. Water-soluble off-on spin-labeled quantum-dots conjugate. *Small (Weinheim An Der Bergstrasse, Germany)*, 4(6), 2008. ISSN 1613-6829.
- [32] B. N. J. Persson and N. D. Lang. Electron-hole-pair quenching of excited states near a metal. *Phys. Rev. B*, 26:5409–5415, Nov 1982. doi: 10.1103/PhysRevB.26.5409.
- [33] M. Li, S.K. Cushing, Q. Wang, X. Shi, L.A. Hornak, Z. Hong, and N. Wu. Size-dependent energy transfer between cdse/zns quantum dots and gold nanoparticles. *The Journal of Physical Chemistry Letters*, 2(17), 2011. doi: 10.1021/jz201002g.
- [34] M. Riskin, Y. Ben-Amram, Ran T.V., V. Chegel, J. Almog, and I. Willner. Molecularly imprinted Au nanoparticles composites on Au surfaces for the surface plasmon resonance detection of pentaerythritol tetranitrate, nitroglycerin, and ethylene glycol dinitrate. *Analytical Chemistry*, 83(8), 2011. doi: 10.1021/ac1033424.
- [35] E.R. Goldman, I.L. Medintz, and J.L. Whitley. A hybrid quantum dot-antibody fragment fluorescence resonance energy transfer-based TNT sensor. *J. Am. Chem. Soc.*, 2005. ISSN 0002-7863. doi: 10.1021/ja043677l.
- [36] Y.T. Yew, A. Ambrosi, and M. Pumera. Nitroaromatic explosives detection using electrochemically exfoliated graphene. *Scientific Reports*, 2016. doi: 10.1038/srep33276.
- [37] T.W. Chen, Z.H. Sheng, K. Wang, F.B. Wang, and X.H. Xia. Determination of explosives using electrochemically reduced graphene. *Chemistry*

- *An Asian Journal*, 6(5), 2011. ISSN 1861-471X. doi: 10.1002/asia.201000836.
- [38] P. Wang, Z.G. Liu, X. Chen, F.L. Meng, J.H. Liu, and X.J. Huang. UV irradiation synthesis of an au-graphene nanocomposite with enhanced electrochemical sensing properties. *J. Mater. Chem. A*, 1, 2013. doi: 10.1039/C3TA11155E.
- [39] H. Kelker, G. Töulg, H. Güünzler, and A. Williams. *Analytical Chemistry: Purpose and Procedures*. Wiley-VCH Verlag GmbH, 2008. ISBN 9783527618323. doi: 10.1002/9783527618323.
- [40] Dengyu Pan, Jingchun Zhang, Zhen Li, and Minghong Wu. Hydrothermal route for cutting graphene sheets into BlueLuminescent graphene quantum dots. *Adv Mater*, 22(6), 2010. doi: 10.1002/adma.200902825.
- [41] Wikipedia. UV-VIS spectroscopy, 2016. URL [https://en.wikipedia.org/wiki/Ultraviolet\T1\textendashvisible_spectroscopy](https://en.wikipedia.org/wiki/Ultraviolet%20textendashvisible_spectroscopy). [Online; accessed 25-10-2016].
- [42] D. Harvey (DePauw University). Photoluminescence, analytical chemistry textbook. URL http://chemwiki.ucdavis.edu/Core/Analytical_Chemistry/Analytical_Chemistry_2.0/10_Spectroscopic_Methods/10.6%3A_Photoluminescence_Spectroscopy.
- [43] R. M. Silverstein and F. X. Webster. *Spectrometric Identification of Organic Compounds - 6th edition*. John Wiley & Sons, Inc., 1998. ISBN 978-0471134572.
- [44] J.S. Gaffney, N.A. Marley, and D.E. Jones. *Characterization of Materials*. John Wiley & Sons, Inc., 2002. ISBN 9780471266969.
- [45] K. Lu. *Nanoparticulate Materials: Synthesis, Characterization, and Processing*. John Wiley & Sons, Inc., 2012. ISBN 9781118408995. doi: 10.1002/9781118408995.
- [46] J.W. Moran and S Bell. Skin permeation of organic gunshot residue: implications for sampling and analysis. *Analytical chemistry*, 2014. ISSN 0003-2700. doi: 10.1021/ac501227e.
- [47] R.K. Biroju, G. Rajender, and P.K. Giri. On the origin and tunability of blue and green photoluminescence from chemically derived graphene: Hydrogenation and oxygenation studies. *Carbon*, 2015.
- [48] J. Ke, X. Li, Q. Zhao, Y. Hou, and J. Chen. Ultrasensitive quantum dot fluorescence quenching assay for selective detection of mercury ions in drinking water. *Scientific reports*, 2014. doi: 10.1038/srep05624.
- [49] X.T. Guo, Z.H. Ni, C.Y. Liao, H.Y. Nan, Y. Zhang, W.W. Zhao, and W.H. Wang. Fluorescence quenching of CdSe quantum dots on graphene. 103 (20), 2013. doi: 10.1063/1.4831670.

- [50] Y. Wang and A. Hu. Carbon quantum dots: synthesis, properties and applications. *J. Mater. Chem. C*, 2:6921–6939, 2014. doi: 10.1039/C4TC00988F.
- [51] L. Zhang, Y. Han, J. Zhu, Y. Zhai, and S. Dong. Simple and sensitive fluorescent and electrochemical trinitrotoluene sensors based on aqueous carbon dots. *Analytical Chemistry*, 87(4), 2015. doi: 10.1021/ac5043686.
- [52] L. Fan, Y. Hu, X. Wang, L. Zhang, F. Li, D. Han, and Z. Li. Fluorescence resonance energy transfer quenching at the surface of graphene quantum dots for ultrasensitive detection of TNT. *Talanta*, 2012.

A Appendix A, Synthesis of rGO

Monolayer graphene oxide (GO) powder, L-ascorbic acid (AA), ACS reagent grade and Ammonia (25 wt. %) was purchased from Sigma Aldrich. An adapted version of the synthesis method described in [26] was used: GO was suspended in DI water and ultrasonicated for 10 minutes. Thereafter, the sample was centrifuged at 8000 rpm for 10 minutes. The supernatant was recovered and the pH was tuned to 9-10 with the addition of ammonia. AA was added and the solution was heated in a waterbath and stirred with magnets. The resulting rGO was centrifuged under the same conditions as before.

Four batches were made before achieving the wished for results. Figure A.1 shows some of the samples from a batch of rGO.



Figure A.1: A batch of rGO samples.

The concentration of GO (mg/L), AA (M), temperature and time under heating/stirring were tuned by varying the different parameters until fully reduced rGO was obtained. The rGO was considered fully reduced when the UV-VIS absorption peak moved from 230 nm (GO) to 270 nm (fully reduced rGO). This was achieved for the following recipe:

- GO concentration: 0.1 mg/mL DI water
- pH adjusted to 10 with Ammonia

- AA concentration: 1-2 mM AA
- Temperature of waterbath: 90 °C
- Reduction time: 30 minutes

Details about the different batches are shown in the table below.

Batch	GO conc. (mg/mL DI)	L-AA conc. (mM)	Temp (°C)
1	0.2	0.5	85
2	0.2	1	90
3	0.1	1	90
4	0.1	1	90

B Appendix B, Synthesis of GQDs

Approximately 10 wt % of glucose (D-(+)-Glucose ACS reagent) was dissolved in DI water. 2 ml of the solution was put in a 20 ml glass bottle with a plastic lid lined with teflon. Capton tape was used to further seal the bottle. The taped bottle was placed in the middle of a conventional microwave, set to medium or medium high effect. The microwave time was varied between 4 and 8 minutes. Before choosing the glass bottle combined with Capton as the vessel for the synthesis process, several materials were tried. Figure B.1 shows some of the container solutions that were tested in the microwave. The final solution included Capton tape and 30 ml bottles with white lids. The lids with the largest thread count were chosen, as these were assumed to hold the highest pressure.

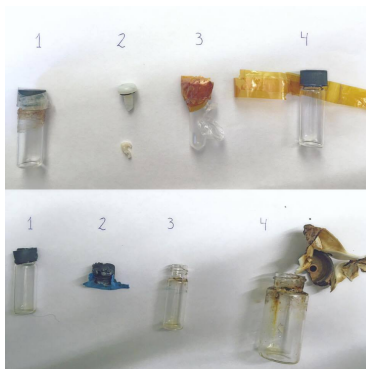


Figure B.1: Microwaved containers.

Figure B.2 shows the fluorescence of the synthesized GQDs compared to the original glucose solution under UV-light.



Figure B.2: Fluorescing GQDs under UV-light. Drops from two different batches, and glucose solution furthest to the right.

C Appendix C, Instruments

C.1 FTIR

FTIR measurements were done with a Vertex 70 V FTIR Spectrometer from Bruker. An MIR source ranging from 400 to 4000 cm^{-1} was used. Measurements were done in reflectance and transmission mode, with double-polished Si or gold as substrate, respectively.

The light source was a MIR, and the detector was a RT-DLaTGS. The spectrum of the source is shown in figure C.1.

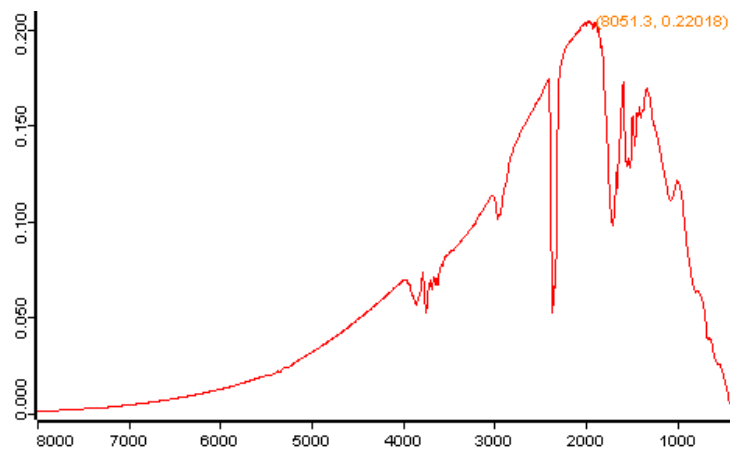


Figure C.1: Intensity of the MIR light source in the FTIR.

Several scans were done to test the machine and setup. Firstly, a background scan was done for vacuum, and a second background scan was done to check the noise level, see figure C.2. This was repeated after one minute. The resulting noise levels were low, but a certain temperature drift could be noticed.

Background scans were then done for the double polished Si substrates used for dropcasting the QD solution. The resulting spectra are in figure C.2. The first

measurement shows a small level of noise, which is almost gone in the second reference measurement. The third measurement, done after the experiments, show a large drift. I think this is due to a change in temperature, and the conclusion is that the time delay between closing the lid of the machine and doing the measurements should be the same in each series.

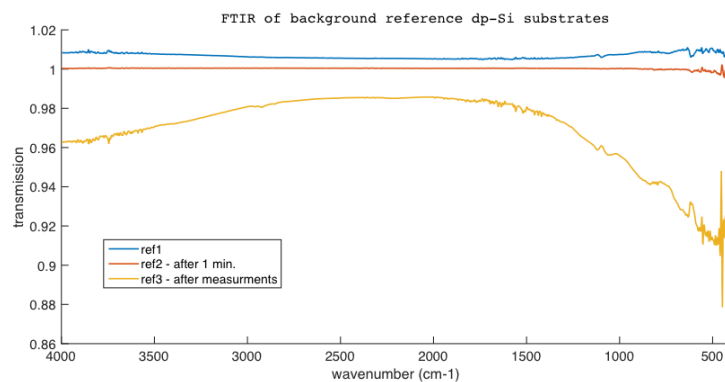


Figure C.2: Reference spectra of substrate.

A test of the paper used as sample holder resulted in zero transmittance. The clear tape used on the side of the sample holder, and the blue tape used for fastening the samples resulted in the spectra in figure C.3. The conclusion is that it is very important to keep the tapes away from the beam line.

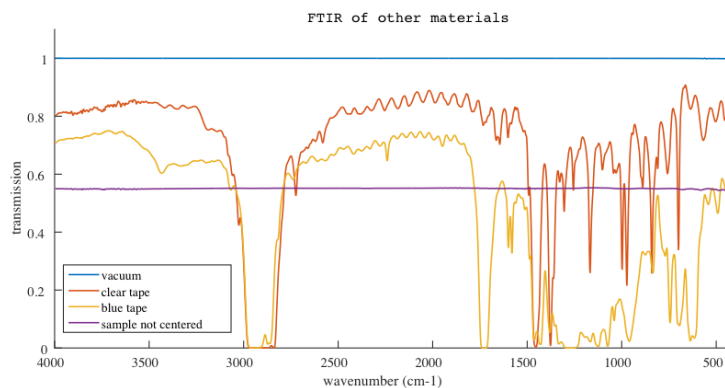


Figure C.3: FTIR of other materials used during the measurements.

There is quite a lot of noise in all measurements for wavenumbers below 1000 cm^{-1} and above 3500 cm^{-1} .

C.2 UV-VIS

The UV-VIS spectrometer used here was a Perkin Elmer Lambda 750. The reference solution for the measurements was DI water.

C.3 PL

PL measurements were done with a Perkin Elmer LS 55. The slits were set to 10 mm to achieve high signals, although this might reduce the resolution a little bit.

C.4 SEM-EDS

The SEM-EDS equipment used in this project was the Zeiss Ultra 55. The substrates were made of Silicon.